Chapter 5
Shape Memory Biomaterials and Their Clinical Applications

Yufeng Zheng, Jianing Liu, Xili Lu, and Yibo Li

5.1 Introduction

Shape memory materials (SMMs) include shape memory alloys (SMAs), shape memory polymers (SMPs), shape memory ceramics, and shape memory composites (SMCs). They are regarded as smart materials with the capability of recovering its permanent shape from a temporary shape under an external stimulus, such as heat, light, pressure, electric field, magnetic field, pH, or solvent. The corresponding shape memory recovering mechanisms are different under different external field.

Shape memory alloy was first discovered by Arne Ölander in 1932, and the term "shape-memory" was first described by Vernon in 1941 for his polymeric dental material [1]. The importance of SMMs was not recognized until William Buehler and Frederick Wang revealed the shape memory effect (SME) in nitinol [1]. Since the orthodontic arch wires developed by George B. Andreasen in 1971, the medical applications of SMAs have been increasing [1], and with the successful application of superelastic nitinol in various mini-invasive surgical tools, and interventional/implantable devices in the last 20 years, nitinol became a unique metallic biomaterial for the designing of medical devices.

The term SMP was first used in 1984 by CDF Chimie Company (France) [2]. However, interest was limited due to the lack of applications in the early days of

Y. Zheng (✉)
Department of Materials Science and Engineering, College of Engineering, Peking University, Beijing, China
e-mail: yfzheng@pku.edu.cn

J. Liu
Academy for Advanced Interdisciplinary Studies, Peking University, Beijing, China
e-mail: jnliu@pku.edu.cn

X. Lu · Y. Li
Institute of Materials Processing and Intelligent Manufacturing, College of Materials Science and Chemical Engineering, Harbin Engineering University, Harbin, China

SMPs. Many SMPs are naturally biocompatible and even biodegradable. Lendlein and Langer reported that SMPs may be used as self-tightening sutures for minimally invasive surgery in 2002 [2], raising much interest for SMPs in biomedical applications consequently.

There is an international organization on Shape Memory and Superelastic Technologies (SMST) found in 1992. In 2004, SMST became an Affiliate Society of ASM International, the worldwide society for materials information. Over a decade, the joint SMST–ASM association has produced many successful conferences, launched a new journal *Shape Memory and Superelasticity*, and created the SMST Graduate Fellowships.

Shape memory effect (SME) is a phenomenon, in which a material recovers its original shape at the presence of the right external stimulus, such as light, electric, temperature, moisture, and magnetic field. For SMAs, they have one-way, two-way, and all-round SMEs, whereas for SMPs, they have multiple SME. Superelasticity (SE in alloys) or viscoelasticity (in polymers) is another important phenomenon, commonly observed under certain conditions. A SMA with superelasticity might be regarded as realizing shape recovery immediately without temperature change, only due to instability of their structure. The shape memory effect is very close to superelasticity phenomena (also named "pseudoelasticity"). The difference of these two definitions might be interpreted in the following way: superelasticity (or pseudoelasticity, which is seemed better in terminological sense) shows us the type of deformational behavior, traditionally relating to elastic one. On the other hand, shape memory denotes the possibility of body made of SMA materials, return to the old configuration. For all SMMs, in general, we need to fix the shape "being recovered by SME or superelastic property" by a treatment/procedure, technically called "shape setting" for SMAs and "programming procedure" for SMPs. Today, a wide range of SMMs have been developed in bulk solid (plate, wire, tube), film, fiber, and even foam shapes.

This chapter aims at providing readers with an overview into the biomedical applications of shape memory materials. It would be divided into four main sections: Section 5.1 is a brief introduction. Section 5.2 provides a summary of the technical background of shape memory alloys. Section 5.3 discusses typical shape memory polymers for biomedical applications. Section 5.4 presents some major conclusions and outlook on future research direction of shape memory materials.

5.2 Shape Memory Alloys (SMAs) and Their Clinical Applications

5.2.1 Fundamental Features of SMAs

Shape memory alloys (SMAs) are a group of metallic alloys that can return to their original form (shape or size) when subjected to a memorization process between two transformation phases, which is temperature or magnetic field dependent. This transformation phenomenon is known as the shape memory effect (SME).

1. Shape memory effect (SME)

Figure 5.1 presents the mechanism of shape memory effect (SME). It can be seen that the SMAs could exist in two different phases (martensite and austenite) with three different conditions, that is, twinned martensite, detwinned martensite, and austenite. The martensite and austenite phases are respectively stable at lower and higher temperature. During heating process, the phase transformation of SMA occurs from martensite to austenite phase. The austenite-start-temperature (A_s) and the austenite-finish-temperature (A_f) are respectively the temperature at which this transformation starts and finishes. Inversely, during cooling process, the phase transformation of SMA occurs from austenite to martensite phase. The starting and finishing temperatures of this transformation are respectively martensite-start-temperature (M_s) and martensite-finish-temperature (M_f). Hysteresis is generally defined as the difference between temperatures at which the materials are in 50% transformed to austenite upon heating and in 50% transformed to martensite upon cooling [3]. Generally, the transformation temperature hysteresis in SMAs is between 10 and 50 °C.
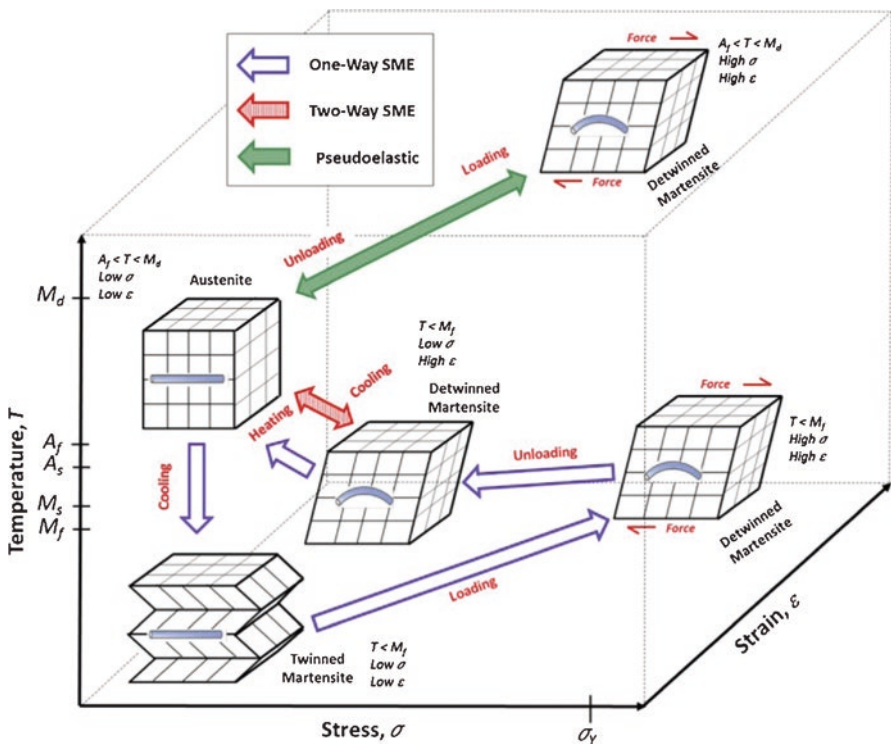

Fig. 5.1 A description of shape memory effect—one-way shape memory effect, two-way shape memory effect, and pseudoelasticity [1]

The SME of SMAs mainly includes one-way shape memory effect (1W-SME) and two-way shape memory effect (2W-SME). As for one-way SMA (1W-SMA), it could retain a deformed state after the external force is removed and recover back to its original shape after heating. As for two-way shape memory effect (also called "reversible SME"), the alloy could recover its shape at both high and low temperatures. However, the strain deterioration of the two-way SMA (2W-SMA) is quick, especially at high temperatures. Thus, the commercial use of 2W-SME is less than the 1W-SME, which is more reliable and economical.

2. Superelasticity

Superelasticity (SE), or pseudoelasticity, is an elastic (reversible) response of SMAs to an applied stress, caused by a phase transformation between the austenite and martensite phases. Unlike the shape memory effect, SE occurs without a change in temperature. In general, SE takes place at sufficiently high temperature where stable austenite phase exists and the SMA is in its parent phase and original shape. When a mechanical strain is imposed, it could stimulate the transformation of an austenite phase to a stable detwinned martensite phase, sometimes called "stress-induced martensitic transformation." SE describes the nonlinear recoverable deformation behavior of SMAs at temperatures above the A_f, including the stress-induced martensitic (forward) transformation in loading and the spontaneously thermally induced austenitic (reverse) transformation upon unloading. The SMA immediately returns to its original austenite phase.

The pseudoelastic behavior of SMA could be significantly influenced by the heat treatment methods. Taking Ti-50.9 at.% Ni alloy as example, Jiang et al. [4] investigated the pseudoelastic deformation behavior after aging treatment at different temperature. It came out that with increasing aging temperature, the temperature window for pseudoelasticity reduces, as shown in Fig. 5.2 [4]. Fundamentally, the effect of aging treatment on pseudoelastic behavior of Ti-50.9 at.% Ni alloy is attributed to its phase transformation behavior. According to Figs. 5.3 and 5.4 [5], with different aging temperature and aging time, the microstructure of Ti-50.9 at.% Ni alloy evolves, and mainly divides into five stages, each of which corresponds to different transformation behaviors [5].

The stress–strain diagrams of three different materials are schematically compared in Fig. 5.5 [1]. In the case of stainless steel, the recoverable strain is less than 0.5%. On the other hand, up to 8% of deformation is recoverable in TiNi SMA. Similarly, bone exhibits more than 1% recoverable strain as well as hysteresis in the loading–unloading cycles. This similarity between deformation behavior of TiNi SMA and bone illustrates the biomimetic behavior of load bearing TiNi SMA implants under loading–unloading conditions in the body. This property highlights another aspect of the excellent biomechanical compatibility of TiNi SMA. Moreover, TiNi SMA exhibits unique corrosion behavior after deformation in superelastic and plastic regimes in different deformation modes [1].
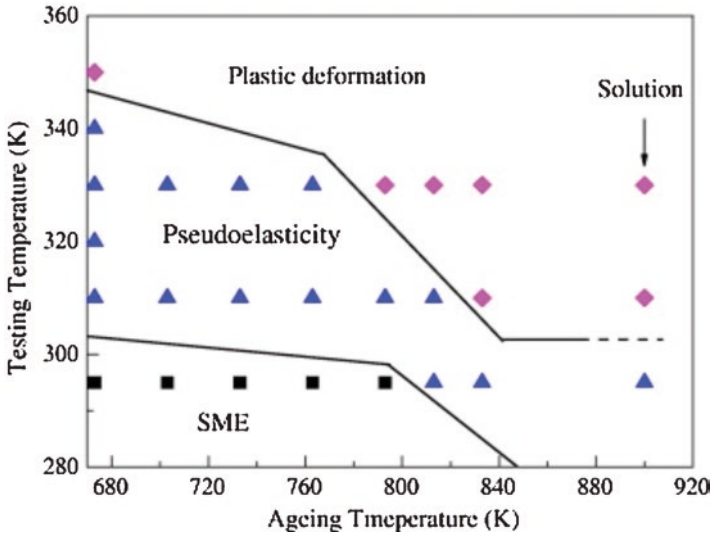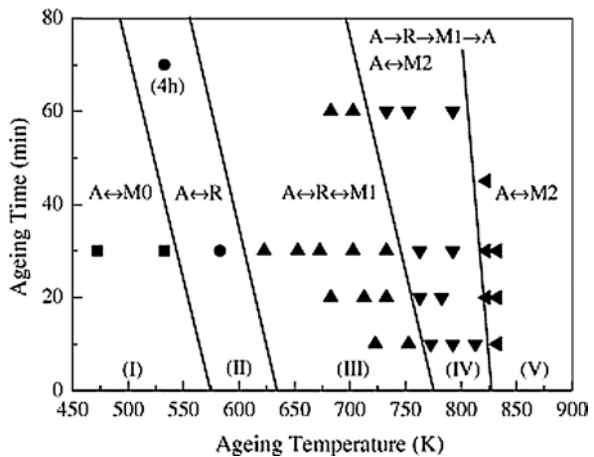
Fig. 5.2 Pseudoelastic deformation diagram of Ti-50.9 at.%Ni [4]

Fig. 5.3 "TTT" diagram illustrating the effect of aging temperature and time on the transformation behavior of Ti-50.9 at.% Ni alloy [5]. (M0, M1, and M2, respectively, denote the martensite formed from the original solutionized B2 phase, R phase, and the aged and precipitated B2 matrix)

5.2.2   TiNi SMAs and Their Clinical Applications

Titanium–nickel alloys, or nitinol (The term "NITINOL" was coined from its composition and its place of discovery: Nickel-Titanium-Naval Ordnance Laboratory.), an equiatomic alloy of titanium and nickel with shape memory and superelastic properties, was discovered in the early 1960s by Buehler and his coworkers [1]. It is an attractive alloy for biomedical application due to its unique functional properties including shape memory effect, superelasticity, biocompatibility, kink resistance, MRI compatibility, and so on.
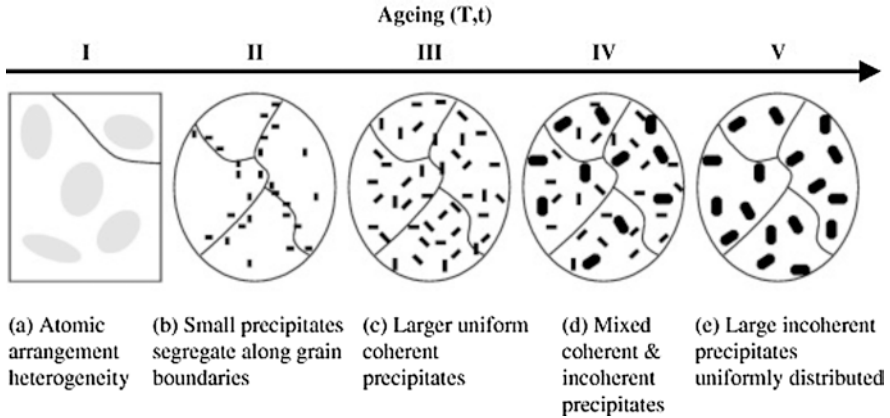
Ageing (T,t)

I   II   III   IV   V

(a) Atomic   (b) Small precipitates (c) Larger uniform (d) Mixed   (e) Large incoherent
arrangement   segregate along grain   coherent   coherent &   precipitates
heterogeneity   boundaries   precipitates   incoherent   uniformly distributed
                                                               precipitates

Fig. 5.4 Mechanisms of the evolution of transformation behavior of NiTi during aging [5]

Fig. 5.5 Stress versus strain relationship for superelastic nitinol, stainless steel, and bone and tendon tissues [1]
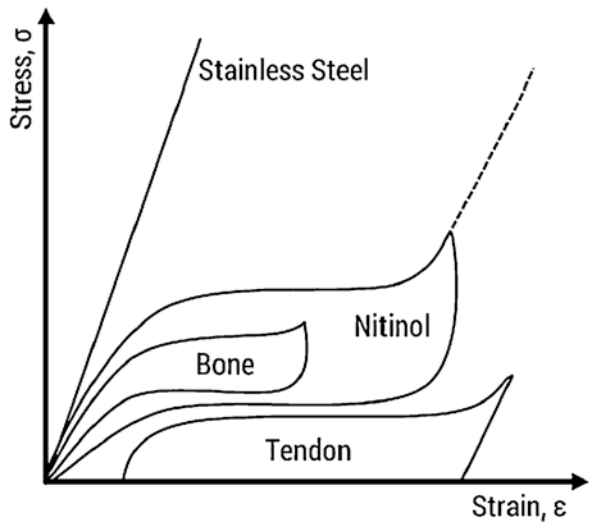
TiNi alloy can be readily deformed by applying an external force and would recover to its original form when heated beyond a certain temperature either by external or internal heating (Joule heating). The main composition range of the TiNi SMA lies in the equiatomic range in Ti–Ni binary phase diagram, in which TiNi alloy stays at intermetallic condition. During fabrication, especially the casting procedure, impurity elements carbon and oxygen are contaminants that must be eliminated from the system. They can affect the mechanical properties and have an impact on the transformation temperature. Thanks to its moderate solubility range, the composition of the TiNi SMA can be changed, and it can be alloyed with other elements to alter both mechanical and shape memory properties. The most general way of modifying nitinol alloy is by including additional nickel up to an extra 1%.

This process not only increases the yield strength of the austenitic phase but also brings down the transformation temperature.

TiNi SMAs have been introduced into the medical implant field for their superelastic and shape memory properties, despite related drawbacks associated with toxic Ni ionic release. TiNi SMA implantable devices such as stents, bone plates, spinal rods, artificial dental roots, staples, clamps, springs, intramedullary rods, heart valves, collapsible valves, artificial anal sphincters, spine rods, graspers, and vena cava filters had been widely used in clinic [3, 6]. In addition to implants, the medical applications of TiNi SMA include orthodontic wires, guide wires and catheters, laparoscopy tools, needles, tissue ablation devices, suture passers, retractors, scissors, and dental drills for root canal procedures [3, 6]. Shape memory effect is advantageous for use in bone plates, staples and thermally activated archwire, while the superelastic behavior is useful in all of the other abovementioned medical devices. Superelastic behavior is becoming the most important property of TiNi SMA with regard to implant devices. Here, the clinical applications of TiNi alloys, mainly focusing on dentistry, orthopedics, and medical intervention, are introduced in the following paragraphs.

5.2.2.1 Application of TiNi SMAs in Dentistry

With regard to dental application, TiNi alloys are always fabricated into orthodontic archwire, root canal instrument, and dental abutment prostheses.

1. Orthodontic archwire. As is known to us, orthodontic wires are used for the correction of arch-oral. During the therapy, forces are applied to teeth and the non-aligned teeth would move slowly. Compared with the traditional stainless steel wires, the TiNi wires would allow the movement of teeth under more constant force over a long treatment with a larger displacement. In the early period, Andreasen [7] investigated the feasibility of cobalt-substituted nitinol wire for orthodontics. The results showed that the nitinol wire, which possessed good elasticity and resistance to corrosion, is suitable for orthodontic use. Besides, Torrisi et al. [8] carried out a series of experiments including dynamic mechanical thermal analysis (DMTA), DSC, tensile test, morphological observation, and microanalysis in order to evaluate the feasibility of TiNi alloy as orthodontic wire. It came out that the orthodontic wire would get improved if the TiNi alloy which provides a constant physiological force on the malocclusion correction of teeth could be adopted instead of the traditional stainless steel. Nowadays, the TiNi orthodontic wire has been developed into orthodontic wire (Fig. 5.6) and used in dentistry. Moreover, orthodontic open spring and close spring made of superelastic TiNi alloys are assistive devices.
2. Root canal instrument. Although the application of the TiNi alloy as a root canal preparation instrument has been over 25 years, the manufacturing strategies diversified only in recent years. For example, the tips of the root canal instrument were previously divided into cutting, noncutting, and partially cutting, while the

current file tips are rounded and noncutting, as is shown in Fig. 5.7 [9]. As for the cross section, the design of which directly determines the cutting ability of a rotary instrument, most current files have triangular or quadrangular cross sections and thus result in negative rake angle. For better innovations of TiNi root canal instrument's design, it is important to modify the basic properties of TiNi alloys, which is greatly influenced by heat treatment methods. As for the clinical outcomes of root canal therapy, Cheung et al. [10] compared the NiTi rotaries with stainless steel file, and it came out that the former showed significantly better periapical outcomes.

3. Dental abutment prostheses. It is reported that the TiNi alloy could be applied for complete arch guided implant treatment [11, 12]. Since the screw- and cement-based retention mechanisms which are used to attach prostheses to dental implants could cause clinical complications (e.g., crown fracturing, peri-implantitis, etc.), Shah et al. [12] proposed an innovative retention system on posterior tooth restorations, as can be seen in Fig. 5.8. As for the abutment system, nitinol was adopted as a shape memory sleeve, which could be activated by temperature change and allow the reversible switch of the device between unlock and lock states. When flaps set to locked position, the crown is retained by sleeves and provides secure and stable retention of prosthesis on implant. According to up to 6 months' follow-up, it came out that the differences between baseline and endpoint assessment of the plaque and gingival indices, probing depth, and proximal and occlusal contacts were minimal. Therefore, it is believed that such nitinol-based retention system is suitable for implant prosthodontics.

5.2.2.2   Application of TiNi SMAs in Orthopedics

Compared with the traditional internal fixation materials used in orthopedics, the TiNi shape memory alloys exhibit superelasticity, good bio-conformity, and high fatigue resistance performance. Therefore, the TiNi alloys have been widely used in

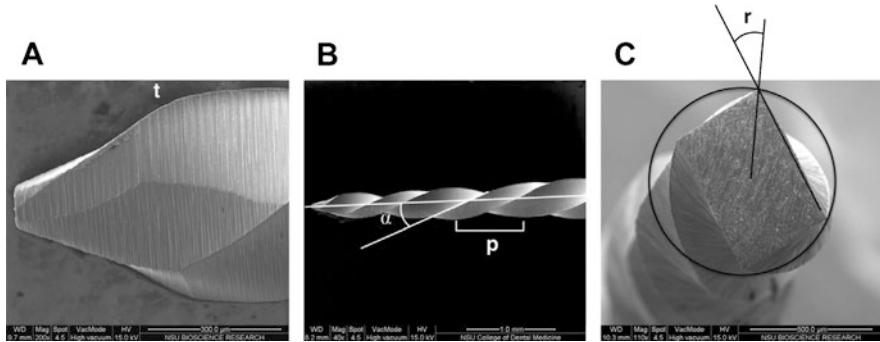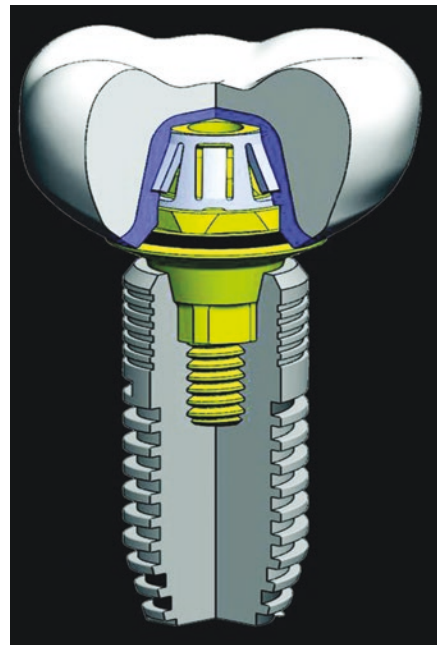**Fig. 5.6** Orthodontic wires made of TiNi alloy

Fig. 5.7 Scanning electron micrographs of an innovative TiNi root canal preparation instrument. (**a**) tip design (**b**) lateral aspect (**c**) cross-sectional design [9]

Fig. 5.8 Schematic diagram of abutment system [12]

orthopedics, such as the arthrodesis concentrator, embracing clamp, staple, bone plate, and so on. Next, the application of TiNi alloys in orthopedics is introduced in detail.

The usage of TiNi SMA as staple for orthopedics application has been reported. Willmott et al. [13] adopted the TiNi SMA staples with different configurations (Fig. 5.9) for the first metatarsophalangeal joint arthrodesis treatment. It came out that the positioning oblique staples at 45–135° were with improved stability and were as strong as the crossed screw. Besides, Laravine et al. [14] used the shape memory nitinol staple (Qual®) in radial shortening osteotomy. According to the

clinical study of 30 cases, all of the fixation of staples at the osteotomy site was strong enough to fulfill fusion. Schipper et al. [15] employed the nitinol compression staples in foot and ankle surgery. Taking the fixation of pseudo-Jones and Jones fracture fixation as an example (Fig. 5.10), the fifth metatarsal fracture showed healed base postoperatively. The TiNi SMA staple would be appealing for trauma indications since by using such staple, minimal incisions and well-preserved periosteum could be achieved [15].

Porous TiNi alloys have also been applied as intervertebral fusion device and bone tissue scaffold [16–18]. There are many advantages for the biomedical application of porous TiNi alloy. Firstly, it possesses high strength, relatively low stiffness, and high toughness, which are important to prevent deformation or fracture, minimize stress-shielding effects, and avoid brittle fracture, respectively. Secondly, its shape memory behavior could help implant insertion and ensure good mechanical stability within the host tissue. Last but not least, the biocompatibility of TiNi SMA is as good as the conventional porous stainless steel and pure Ti implant materials. The fabrication of porous TiNi SMA could be achieved by powder metallurgy techniques, the commonly used methods of which include self-propagating high-temperature synthesis (SHS), spark plasma sintering (SPS), hot isostatic pressing (HIP) with argon expansion, capsule-free HIP (CF-HIP), and conventional sintering (CS). Figure 5.11 [16] shows the porous NiTi produced by three different methods, that is, (a) SHS, (b) CF-HIP with argon expansion, and (c) MIM and sintering with NaCl space holder. Figure 5.11d shows a porous TiNi implant (Actipore™, Biothex, Canada) produced by SHS process for intervertebral fusion application. Figure 5.12 [17] shows the product of Actipore™ PLFx and PNT, which has been implanted for over 100 times worldwide. It should be noted that the chemical homogeneity of the porous TiNi SMAs is important for biomedical application. The presence of secondary Ti- and Ni-rich phase is undesirable with regard to its biocompatibility. In order to solve this problem, Bertheville et al. [18] used vapor phase calciothermic reduction process during the formation of NiTi compound. The sintered porous NiTi is shown in Fig. 5.12d [18]. It came out that the single-phased NiTi with superior chemical homogeneity is applicable for bone graft substitute.

Fig. 5.9 Shape memory TiNi staples [13]

Fig. 5.10 Preoperative (**a**) and postoperative (**b**) image of the fifth metatarsal fracture [15]

In addition, TiNi SMAs have been fabricated into arthrodesis concentrator (Fig. 5.13), embracing clamp (Fig. 5.14), and bone plate (Fig. 5.15) for the treatment of carpal collapse [19], complex femoral revision hip arthroplasty [20], and noninvasive alteration of bending stiffness [21], respectively. As for fracture healing, the biomechanical stimulus is important. The alteration of fixation stiffness during healing course, which could be achieved by TiNi SMAs, could accelerate bone healing and prevent healing complications. On the whole, by careful consideration of the interaction between design, materials properties, and manufacturing processes, the TiNi SMAs with optimal properties are suitable for orthopedics applications.

5.2.2.3 Application of TiNi SMAs in Interventional Therapy

As for interventional therapy, the TiNi SMAs have been widely used as stents (including vascular stent and nonvascular stent) and other interventional devices such occluders, filters, and retrieval tools, which will be introduced below.

1. Stents. As is known to us, the endovascular stents could be simply divided into two major subtypes—balloon-expandable stent and self-expandable stent. In virtue of the superelastic property, TiNi SMAs are widely used as self-expandable stent, which could supply chronic outward force (COF) to expand the vessel and
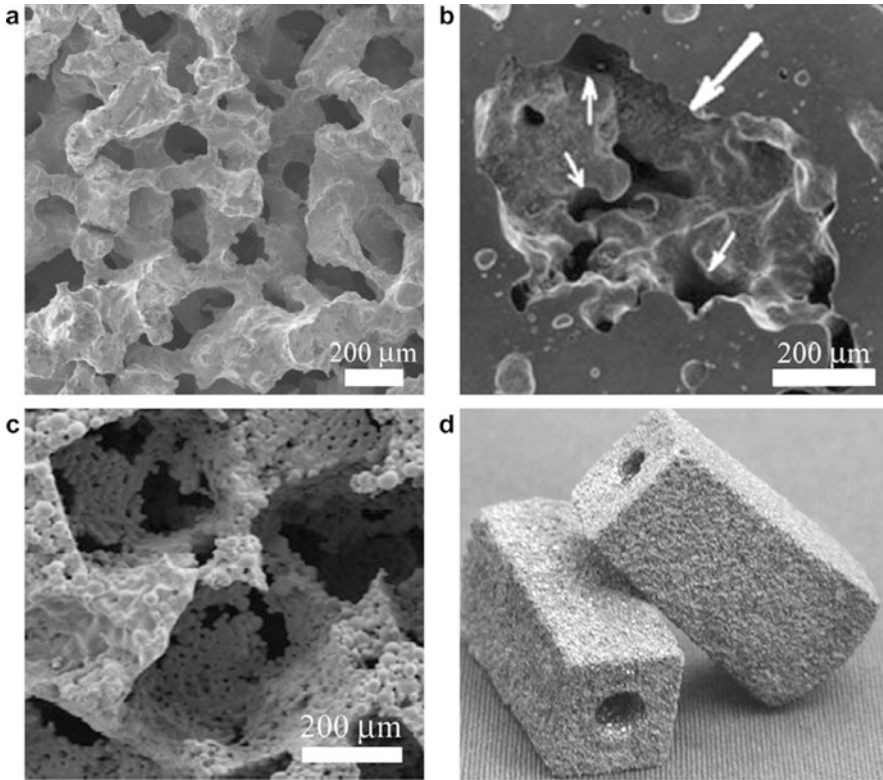
Fig. 5.11 SEM micrographs of porous NiTi produced by (**a**) SHS, (**b**) CF-HIP, and (**c**) MIM. (**d**) NiTi implant for intervertebral fusion application [16]
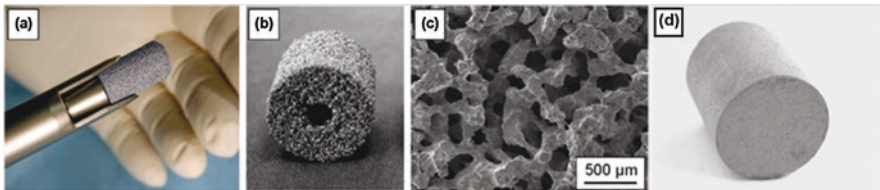

Fig. 5.12 (**a–c**) porous NiTi interbody fusion device Actipore™ produced by SHS [17]. (**d**) Optical micrograph of porous NiTi [18]

elastically recoil after flattening. Unlike the releasing mechanism of balloon-expandable stent, the self-expandable stent is completely compressed within a delivery sheath and needs to be "unsheathed" for placement and delivery. Pre- or post-dilation of self-expandable stent is necessary sometimes due to the lack of stiffness and outward force. As a nitinol self-expandable stent shown in Fig. 5.16 [22], the Supera peripheral stent (Abbott Vascular, Santa Clara, CA) has received the US Food and Drug Administration (FDA) approval. Among the femoropopliteal lesions, the 1- and 2-year primary patency rates were respectively 83–85%

Fig. 5.13 Four-corner arthrodesis concentrator made of NiTi shape memory alloy. (**a**) Apical view, (**b**) lateral view [19]
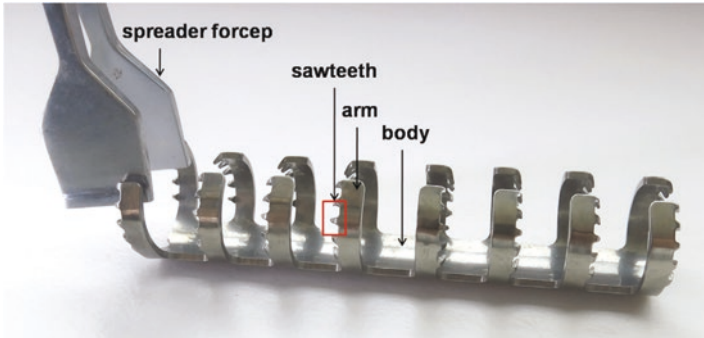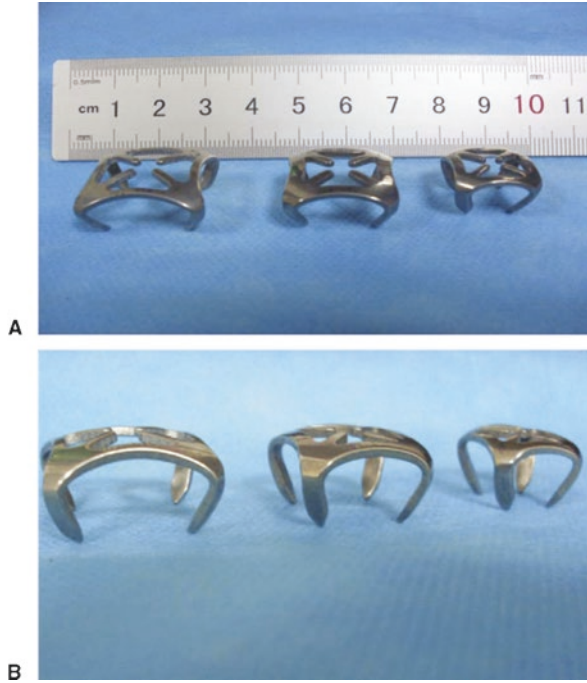

Fig. 5.14 NiTi shape memory sawtooth-arm embracing clamp with a body, pairs of arms, and sawteeth [20]

and 62–76%. No stent fractures occurred in approximately 200 patients according to three independent retrospective studies [23]. Except for Supera stent, other biomimetic nitinol stents are also in R&D stage, such as BioMimics 3D (Veryan Medical Ltd., Horsham, UK), as is shown in Fig. 5.17 [22]

For better understanding the whole procedure of the working mechanism of self-expandable TiNi SMA stent, the stent performance cycle is portrayed on a typical superelastic stress–strain curve, as shown in Fig. 5.18 [6]. First, the TiNi SMA stent
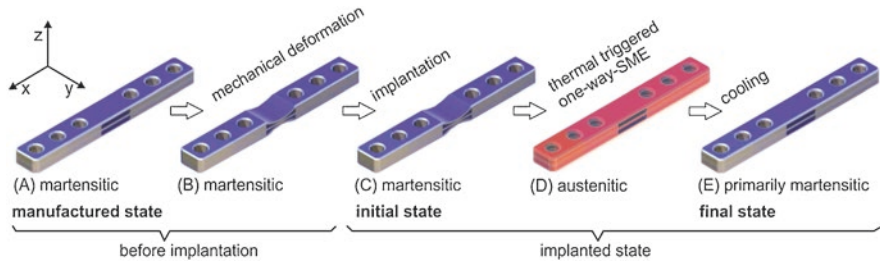
Fig. 5.15 General concept of a shape memory bone plate with alterable stiffness [21]
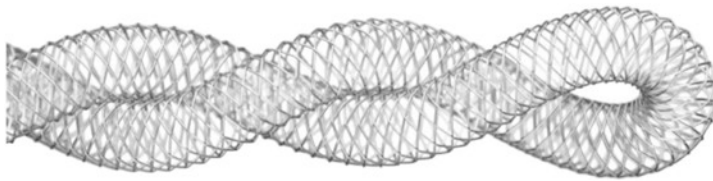

Fig. 5.16 Illustration of Supera stent [22]

is manufactured in expanded diameter (A) and then compressed into a catheter (B). It should be noted that the process from A to B would follow a different path since the deformation process is unlikely to be achieved at body temperature. The TiNi SMA stent would follow the unloading path from B to C after deploying in the body. At point C, the TiNi SMA stent contacts the vessel wall and presents a biased stiffness. The COF against a vessel wall follows the unloading plateau (C to E), while the resistance of the TiNi SMA stent to further compression follows the loading plateau (C to D). If the s TiNi SMA tent is re-expanded to a larger diameter, the filled circle B would shift to the left, while the stiffness would remain unchanged.

Compared with the conventional surgery, the minimally invasive surgery is more technically demanding, because the surgical intervention is within a confined space and remotely controlled via two-dimensional imaging of the operative field. It is known that the stent–graft failure is always induced by stent migration, device fatigue, and the risk of endoleaks. Therefore, it is important to optimize the geometrical structure of stents and evaluate its mechanical properties. Numerical study with finite element analysis (FEA) is an effective way for simulation of mechanical behaviors. By FEA, Zhou et al. [24, 25] developed a novel nitinol endovascular stent–graft system and a new endovascular stent–graft system, respectively, for abdominal aortic aneurysm and type B thoracic aortic dissection with experimental verifications. The images for the former stent graft system and the postoperative therapeutic effect of the latter one are respectively shown in Fig. 5.19 [24] and Fig. 5.20 [25] for brief introduction. On the whole, both stent graft systems received very positive clinical results and showed advantageous therapeutic efficacy.

With regard to nonvascular stent, the TiNi SMAs could be applied as esophageal stent, intestinal stent, tracheal stent, biliary stent, urethral stent, and so on. Similar

Fig. 5.17 3D modeling of
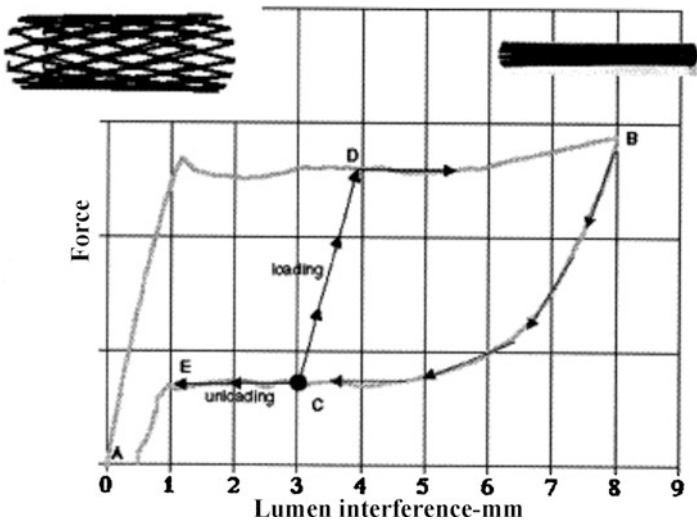the BioMimics 3D helical
stent [22]

Fig. 5.18 The stent performance cycle which is portrayed on a typical superelastic stress–strain
curve [6]

to the endovascular stent, the nonvascular stent made of TiNi SMAs could be self-expandable, in advantage of its SME. Taking the esophageal stent as an example, there are many currently marketed self-expandable metal esophageal stents (SEMS) and self-expandable plastic esophageal stents (SPMS) in the USA. Among those SEMS, TiNi SMAs have become the dominant material, which is benefited from its elasticity, bio-conformity, higher radial resistive forces, as well as SME [26]. It should be noted that the esophageal SEMS were used to be uncovered, leading to rapid tumor or granulation tissue ingrowth. Thus, the partially covered SEMS (Fig. 5.21) have been developed [26]. Only a small portion of the stent is bare TiNi SMAs, which is usually the proximal and distal ends, in order for the embedding of stent into the esophageal wall. It came out that compared with the uncovered group, reinterventions of the partially covered group at 6 months postoperatively are significantly lower in a multicenter prospective randomized controlled trial (RCT) [27].

2. Medical devices used in the treatment of structural cardiac disease. TiNi SMAs have also been applied in the treatment of structural cardiac disease, mainly including the occluder, heart valves, and retrieval toolbox.

The nitinol occluder has been adopted for the treatment of atrial septal defect (ASD), ventricular septal defect (VSD), left atrial appendage occlusion, etc. [28]. Taken the treatment for ASD as an example, it is the second most common congenital heart defect. As for the secundum ASD, transcatheter techniques could be adopted. The Amplatzer septal occluder (Fig. 5.22), which is composed of a self-expanding double disk made of TiNi SMAs with a short connecting waist, is the most commonly used device for closure [28]. It is made of superelastic nitinol wire mesh (0.004–0.008 inch) covering a polyester material for the reduction of blood flow through the device. Since the risks of complications and implantation failure are low [29], the application of the device is reliable.
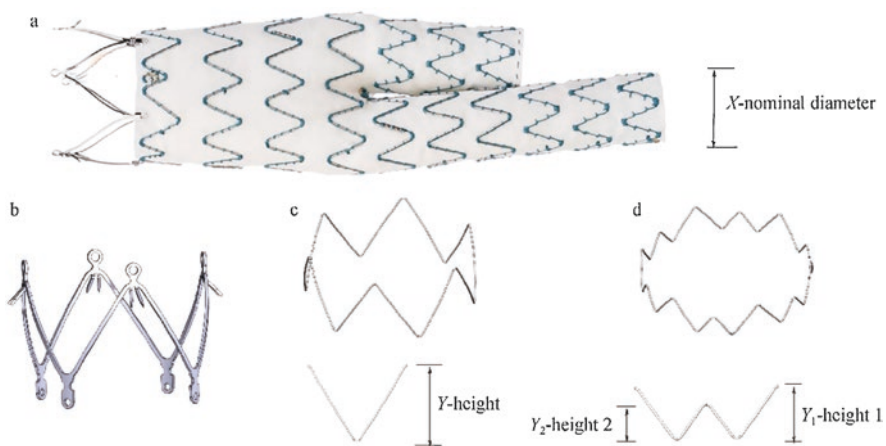

Fig. 5.19 Nitinol endovascular stent–graft and its components. (**a**) full stent graft (**b**) suprarenal stent (**c**) V type stent and (**d**) W type stent. [24]
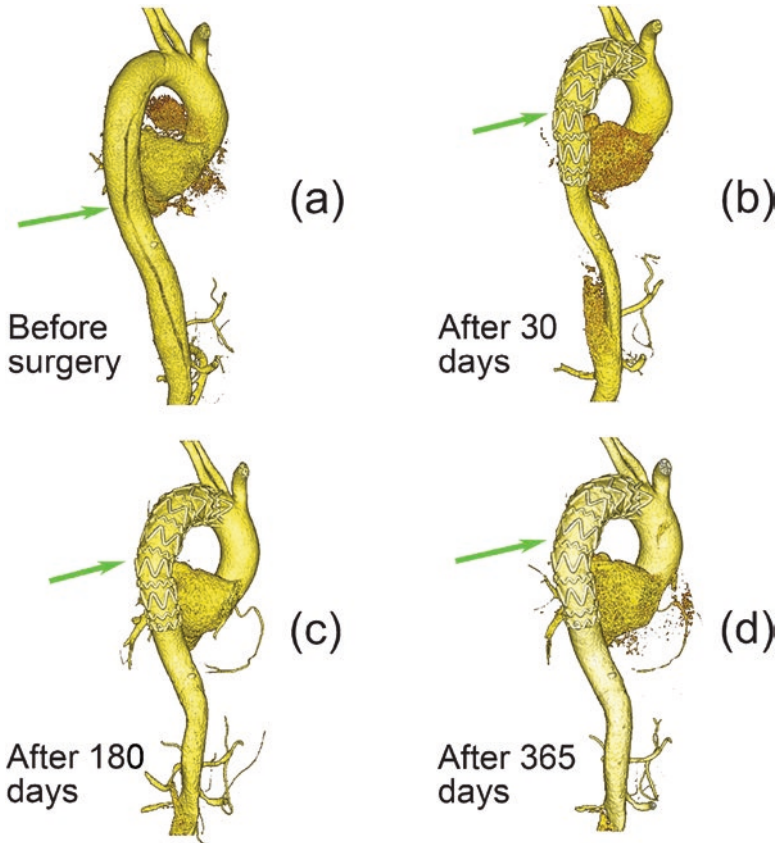
Fig. 5.20 3D CT blood flow results of a patient's thoracic aorta pre and post operation. (**a**) before surgery. (**b**) 30 days (**c**) 180 days and (**d**) 365 days after surgery. [25]

As for the treatment of aortic stenosis, transcatheter aortic valve replacement (TAVR) is one of the commonly used methods, especially for the high-risk patients or those who are not qualified for surgery aortic valve replacement (SAVR). There are many valves for TAVR available in the current market or in development; some of them are based on the self-expanding nitinol frame, such as the CoreValve (Medtronic, Minneapolis, MN, USA) (Fig. 5.23), Portico valve (St. Jude Medical), and so on [28]. Thanks to the self-expanding releasing design, there is no need for rapid pacing during deployment. It is noteworthy that the transcatheter structural interventions might lead to device embolization (DE). As a rare complication of DE, sometimes it would be life-threatening.

Percutaneous retrieval tools are necessary for the management of device embolization. They could be divided into the snare-based devices and non-snare-based devices. As for the latter one, it could also be applied for myocardial biopsies, electrophysiological applications, and interventional radiology procedures, as shown in

Fig. 5.21 Partially
covered SEMS [26]

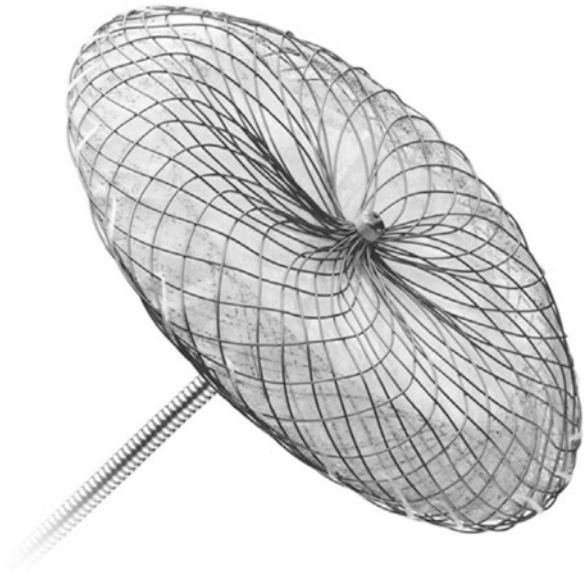**Fig. 5.22** Amplatzer
septal occluder [28]

Fig. 5.24 [30]. In particular, Fig. 5.24c shows a stone extractor (NGage®, Cook Urological Inc., Bloomington, IN, USA) made of nitinol, which could help the physician for the engagement, reposition, release, or extraction of stones in the kidney or ureter.

Pulmonary embolism (PE) is a common and life-threatening disease, especially for elder people. Inferior vena cava (IVC) filter is a kind of vascular filter which is implanted into the inferior vena cava to prevent PE. Among the developed IVC filters, some of them are made of nitinol, such as the Option Elite (Argon Medical Devices Inc., Plano, TX) (Fig. 5.25), Bard Denali (CR Bard, Murray Hill, NJ), and Cordis OptEase (Cordis Corp, Hialeah, FL) filters [31]. All of them are retrievable type filters and also MRI conditional. The OptEase and Denali filters were cleared by FDA, respectively, in 2004 and 2013 [31].

5.2.2.4 Additive Manufacturing TiNi SMAs

In order to meet the need of individual patient, customized design of medical devices is sometimes required, especially for the bone implants. This would be difficult for the conventional manufacturing methods of TiNi SMAs such as machinery, while additive manufacturing (AM) has shown its particular advantages, especially for the combination of dense and porous structures in three dimensions. By AM, each layer of material could be melted in accordance with the geometry defined by a three-dimensional computer-aided design (3D CAD) model. The alteration of 3D CAD models could satisfy the needs for different customized medical devices. Besides, by adding successive layers of material, rather than removing it, the product could be manufactured with little or no waste.

With regard to TiNi SMAs, the commonly used AM techniques are powder bed-based technologies, including selective laser sintering (SLS), direct metal laser sintering (DMLS), selective laser melting (SLM), and LaserCUSING [32]. SLM is a commonly used method for the fabrication of 3D printing TiNi SMA implants. In order to obtain the SLM TiNi alloy with excellent performance and minimal structural defects, it is important to choose optimal laser processing parameters. For

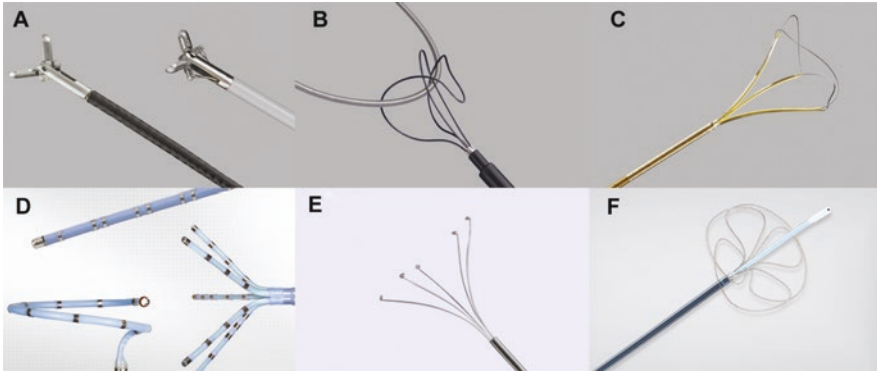**Fig. 5.23** Medtronic CoreValve and delivery sheath [28]

Annulus range 18-29mm
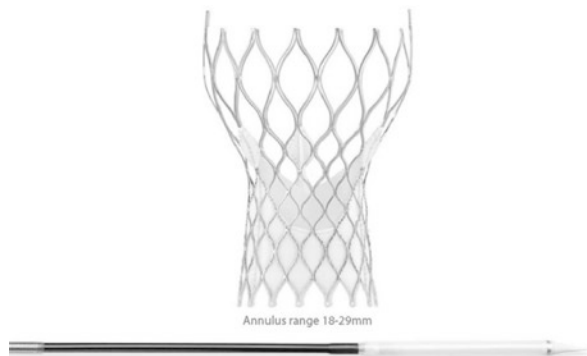
Fig. 5.24 Non-snare-based retrieval systems. (**a**) biospy forceps (**b**) needle's eye retrieval system (**c**) NGage nitinol stone extractor (**d**) adjustable lasso catheters (**e**) captura three-prong graspers (**f**) Indy retriever [30]
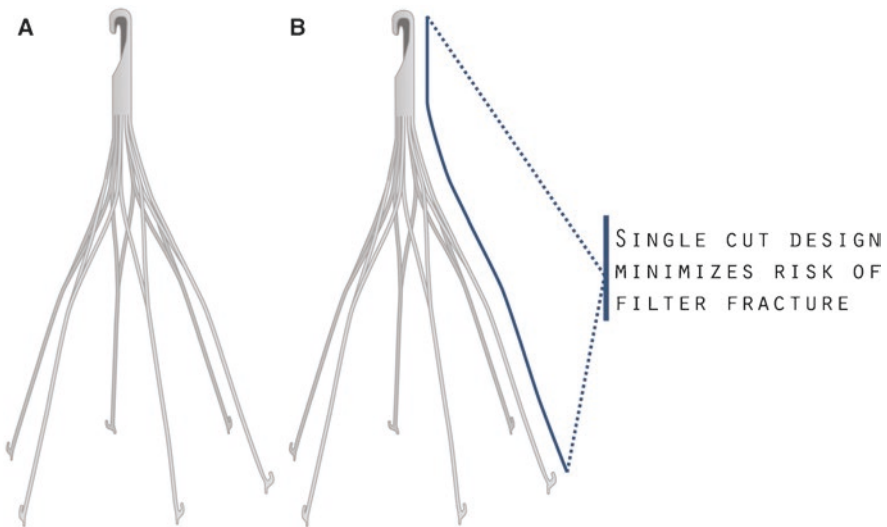

Fig. 5.25 (**a**) Option Elite filters and (**b**) its design explanation. [31]

example, it is reported that a sharp-focused laser beam is more desirable than a divergent focus. As can be seen from Fig. 5.26 [32], the levels of adherent particles within pores decrease significantly by focused laser beam. In order to investigate the feasibility of SLM-TiNi implants for biomedical application, Habijan et al. [33] cultured human mesenchymal stem cells (hMSC) for 8 days on the SLM-TiNi implant and investigated its biocompatibility. It came out that both dense and porous SLM-NiTi implants are suitable carriers for hMSC. The nickel ion releases of SLM-TiNi implants in the cell culture medium were all below the threshold value to cause cytotoxicity. Besides, it is noteworthy that by fabricating the interpenetrating phase

composite, the mechanical performance of 3D printing TiNi implants could be improved.

In 2020, Zhang et al. [34] developed a 3D printing Mg-NiTi interpenetrating phase composite, the shape and strength of which could largely recover by heat treatment. The improved strengths, excellent damage tolerance, satisfactory damping capacities, and exceptional energy absorption efficiency of this composite enable its application in future biomedical fields.

5.2.3   Nickel-Free Ti-Based Shape Memory Alloy

To avoid the unnecessary problem of the toxic Ni ion released during using the TiNi SMA for biomedical application, Ni-free Ti-based biomaterials for use in implant devices are being developed. Unfortunately, the shape memory effect and superelastic property of the developed Ni-free Ti-based biomaterials are not good as nitinol,
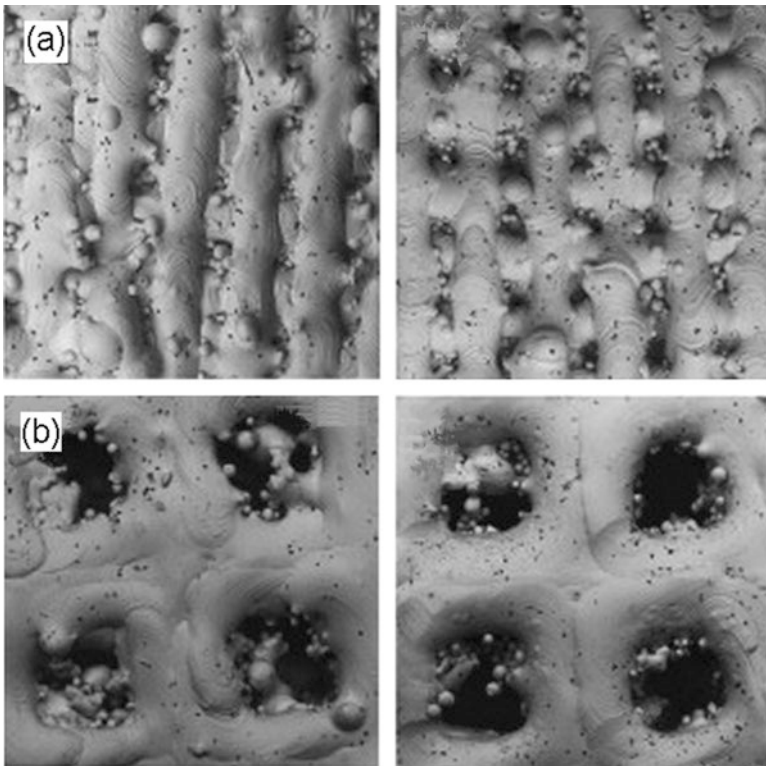

Fig. 5.26 SEM images of NiTi (**a**) porous (12.5%) by large hatch distance and (**b**) porous (34.5%) by engineered porosity. The left images are NiTi fabricated by divergent laser beam, while the right ones are by focused laser beam [32]

and present studies are focusing on further improving their shape memory and superelastic behaviors.

For the origin of the shape memory effect in nickel-free Ti-based SMAs, the dominant mechanism should be the reversible $\beta \leftrightarrow \alpha''$ transformation. In order to design the desired β-Ti alloys with good SME and SE, the d-electron alloy theory is commonly used, the validity of which has been proved for approximate prediction of the stability of different solid solution phases and the elastic modulus. There are two primary parameters in this theory, that is, the bond order (B_0) and the d-orbital energy level (M_d). For different alloying element, both of them are distinctly calculated. The B_0 and M_d values of alloys are respectively denoted as $\bar{B}_0$ and $\bar{M}_d$. Based on this two parameters, another parameter called bonding force (BF) using $\bar{B}_0$ and $\bar{M}_d$ values through Coulomb's law was derived, which represents the bond force between titanium ions and alloying element's ions. It is reported that the parameters $\bar{B}_0$, $\bar{M}_d$, and BF correlate with the superelasticity of β-Ti alloys [35]. Figure 5.27 [35] presents the corresponding $\bar{B}_0$ and $\bar{M}_d$ values of the developed Ni-free superelastic Ti alloys. The average bond force (BF) for the groups is indicated by arrows. According to Fig. 5.27, with increasing $\bar{B}_0$ and $\bar{M}_d$ values along the twin boundary on the map, the BF values decrease.

5.3 Shape Memory Polymers

Shape memory polymers (SMPs) possess the ability to recover their original shape from their temporary shape under external stimulus. Compared with traditional shape memory alloys, SMPs have many advantages, such as lightweight, low-cost, tunable properties (e.g., shape recovery temperature), good shape change (up to 1000% recoverable deformation), and easy processing. Since the first SMP (shape memory polynorbornene) was discovered and commercialized in 1984 [36], many kinds of SMP with different structures have been explored and have been used in different application fields, such as flexible electronic devices [37], sensor and actuators [38], smart textiles and apparels [39], and so on. Furthermore, biodegradable or biocompatible SMPs can be prepared, which enlarge their applications field to clinical applications, for example, devices for minimally invasive surgery, tissue engineering, drug delivery, surgical suture, and so on. Although, compared with SMA, SMPs have outstanding performances in many aspects, they still have inherent shortcomings of low mechanical strength and recovery stress. These problems have largely limited the applications of SMPs. This part presents the general concepts of SMPs and important progress and clinical applications related to SMPs.
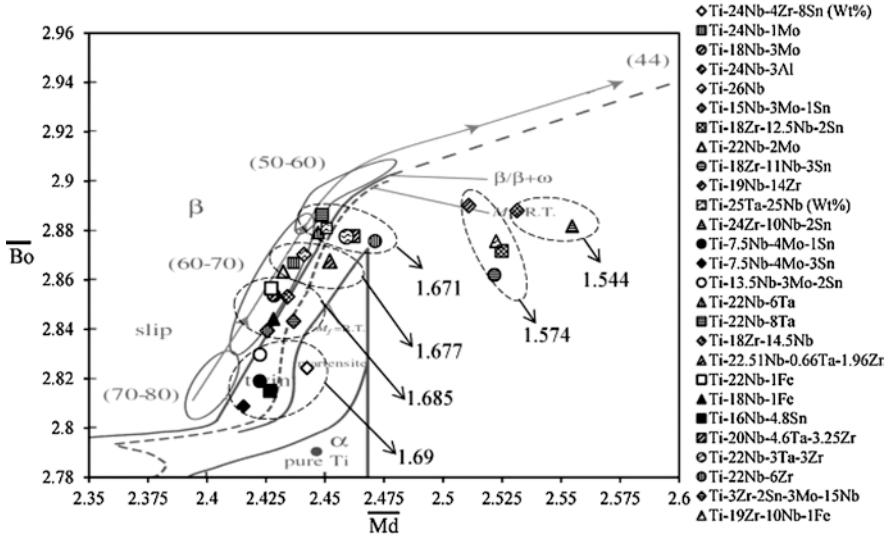
Fig. 5.27 $\bar{B}_0 - \bar{M}_d$ diagram and the average BF values of developed β-Ti alloys [35]

5.3.1   General Mechanism of Shape Memory Polymers

SMPs can be exploited in different polymer systems which have great differences in molecular structure. Generally speaking, SMPs have two-phase structure, i.e., fixed phase and reversible phase [40]. The fixed phase plays an important role in defining the permanent shape and preventing flow deformation of polymer under the application of stress. Both chemical cross-links and physical cross-links can serve as fixed phase. The reversible phase is responsible for controlling the shape retention and recovery under external stimulus. The amorphous, crystalline, supramolecular entities, etc. act as reversible phase in SMPs. Figure 5.28 presents the different molecular structure of the fixed phase and reversible phase. As shown in Fig. 5.28, the fixed phase functions as netpoints, which can be formed by molecular entanglements, crystalline phase, H-bonding, chemical cross-links, and interpenetrating or interlocked supramolecular network. The reversible phase acts as a switch which can be crystallization/melting transition [41], glass transition [42, 43], liquid crystal anisotropic/isotropic transition [44–46], supramolecular association/disassociation [47], and light-reversible coupling groups [48, 49].

From the view of thermodynamics, the shape memory effect (SME) of polymer is a change process from unstable state to stable state. Before deformation, the SMP (in original shape) is in a thermodynamic stable system. After deformation, the SMP (in temporary shape) is in a state of thermodynamic instability. The shape recovery process is a thermodynamic spontaneous process, that is to say, the shape recovery is initiated by entropic elastic force of the polymer network.
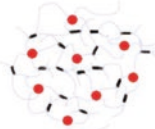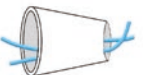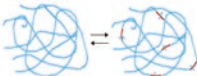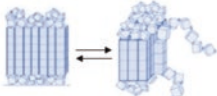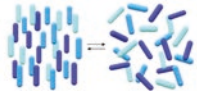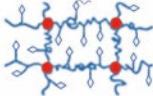
		Molecular entanglement	
Fixed phase	Physical crosslinking	crystalline	
		H-bonding	
	Chemical cross-linking		
	Interpenetrating network		
	Interlocked supramolecular		
Reversible phase	Amorphous phase (glass transition)		
	Crystalline (crystallization/melting transition)		
	Liquid crystalline (anisotropic/isotropic)		
	Supramolecular (association/disassociation)		
	Light-reversible coupling groups		

Fig. 5.28 Various molecular structures of SMPs. Fixed phase and reversible phase are the essential conditions for the SMPs showing SME

5.3.2 Shape Memory Functions

5.3.2.1 One-Way Shape Memory Effect

One-way SME is the most simple and common SME, in which the polymer can change from a temporary shape to a permanent shape under an external stimulus. However, the temporary shape is not recoverable by applying a reverse stimulus. We take the thermal-induced one-way SME as an example to clarify the shape memory effect procedures. The programming procedures contain four steps: (1) SMP is heated above transition temperature (T_{high}) and held a certain time. Then, the sample is stretched to a certain elongation ε_m. During this process, the polymer segments are stretched under external stress because the sample exhibits high elasticity at T_{high}. As a result, macroscopic deformation of the sample (temporary shape) is obtained and the elastic energy is stored. (2) The sample is cooled to below the transition temperature (T_{low}), while the stress is kept constant. The movement of polymer segments is frozen at T_{low}. (3) The sample is then unloaded which results in the retention strain ε_u, which means the temporary shape is fixed. (4) Raising the temperature from T_{low} to T_{high} and maintaining a certain time, the stretched sample can recover to its original shape since the segment mobility is activated and the restoring force is generated because of the release of the stored elastic energy. The recovery strain is recorded as ε_p. The shape fixity ratio (R_f) and shape recovery ratio (R_r) can be calculated according to the following equation:

$$\text{Shape fixity ratio }(\%) = \varepsilon_u \times 100 / \varepsilon_m \tag{5.1}$$

$$\text{Shape recovery ratio} = (\varepsilon_m - \varepsilon_p) \times 100 / \varepsilon_m \tag{5.2}$$

Shape fixity ratio characterizes the ability of the sample to keep its deformation after unloading, and the shape recovery ratio quantifies the ability of the sample to recover its original shape. An additional parameter for evaluating the recovery behavior is recovery stress, which can be recorded during the programming step (4). One-way SME can be affected by different factors, including internal factors such as the segment contents [50–52], the molecular weight, crystallinity of the polymers [53, 54], ionic group contents [55], and external factors, for instance, the amount of pre-deformation, the deformation temperature, and processing conditions [55, 56].

5.3.2.2 Two-Way Shape Memory Effect

Recently, two-way shape memory effect (2W-SME) has attracted wide attention of researchers. Unlike common one-way shape memory effect (1W-SME), these polymers can convert between permanent shape and temporary shape without subsequent programming procedure. 2W-SME was first reported for liquid crystal elastomers [57] and then has been illustrated in different polymer systems. Generally,

there are four molecular structures to prepare the SMPs with 2W-SME. They are 2W-liquid crystalline elastomers [58, 59], semicrystalline 2W-SMPs [60–62], 2W-shape memory composites or laminates [63–65], and 2W-interpenetrating networks [66, 67]. Zare made a comparison between the structures of the four kinds of 2W-SMPs as shown in Fig. 5.29 [68].

Basically, the structure of 2W-SMPs possesses netpoints that maintain a permanent shape and the switching segments for producing a temporary shape. Compared with 2W-SMPs, 1W-SMPs lack the ability of driving the permanent shape to return to the temporary shape. Introducing the internal stress through thermomechanical training can produce 2W-SMP. Thermomechanical training is a physical operation process. In each training cycle, a specific deformation path is selected to realize 2W-SME. By changing the training conditions, various temporary shapes can be changed reversibly.

A typical thermomechanical training is described in Fig. 5.30a. The whole process consists of four steps as shown in the green line (A-B-C-D-E) in the figure. Firstly, the sample is heated above melting temperature of all segments (green line A-B). In this state, the chain segments will undergo reversible high elastic deformation without any flowing. In the second step, the polymer network is deformed at the constant temperature (green line B-C), resulting in a high elastic deformation. Above the melting temperature, the strain recovery caused by the movement of chain segment is consistent with the applied stress. After that, at the third step, cooling down the sample to a low temperature (green line C-D), crystallization will
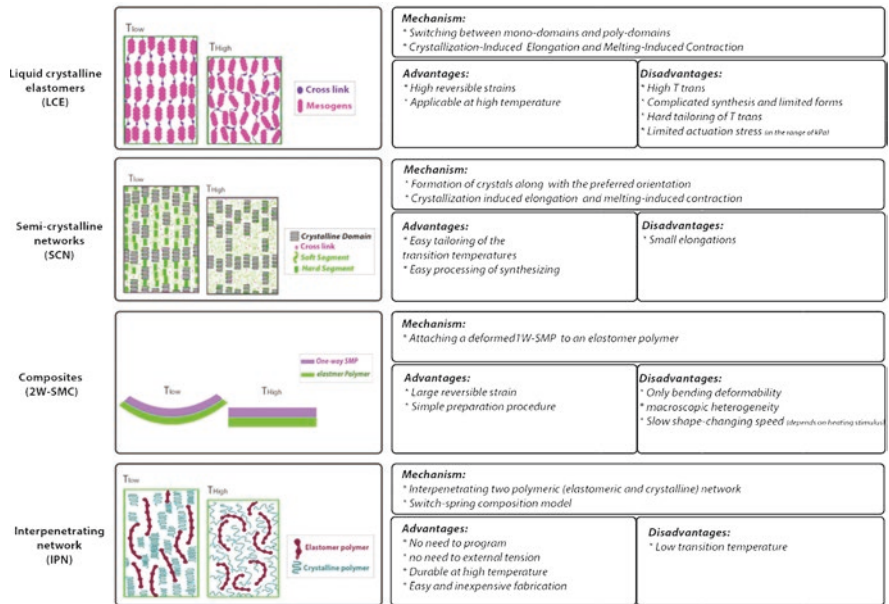

Fig. 5.29 Schematic of the structures, mechanisms, advantages, and disadvantages of the four kinds of 2W-SMPs [68]

occur. Before crystallization, under the action of internal or external stress, the distance of cross-linking point is adjusted to orient the molecular chain. As a result, the conformational entropy of the network decreases at the end of crystallization. The applied stress is removed and the sample obtains a temporary shape. Lastly, in the fourth step, the sample is reheated to high temperature, and it can be seen that the sample returned to its permanent shape, owing to its entropic elasticity (green line D-E). The 2W-SME is verified by the purple line, in which the sample is heated to the melting temperature and then cooled down to low temperature. Figure 5.30b shows the cyclic behavior of a 2W-SMP based on the temperature variation. The TMA result indicates that the 2W-SME tends to be consistent after four cycles.

2W-SME is a necessary requirement for some applications such as sensors, actuators, artificial muscles, and so on. However, the design and fabrication of 2W-SMPs are still a challenge and require constant efforts. The focus of future research is still on exploring new types of netpoints and switching segments. In addition, developing nonthermal-induced 2W-SMPs is an important research direction. 2W-SMPs have wide application, and its biomedical applications are the main focus of current research.

5.3.2.3 Triple Shape Memory Effect

Triple-shape memory effect (TSME) means that a polymer can be deformed into two temporary shapes and then can recover to its permanent shape in steps under stimulation. Compared with the traditional 1W-SME, TSME can achieve more complex recovery actions.

TSME is based on the polymer with two separated transition temperatures or one broad transition temperature. Two separated transition temperatures can be two melting transitions [69, 70], one glass transition and one melting transition [71], two glass transitions [72], and one glass transition and one liquid crystalline transition [45, 73, 74]. Figure 5.31 shows the molecular mechanism of TSME for a
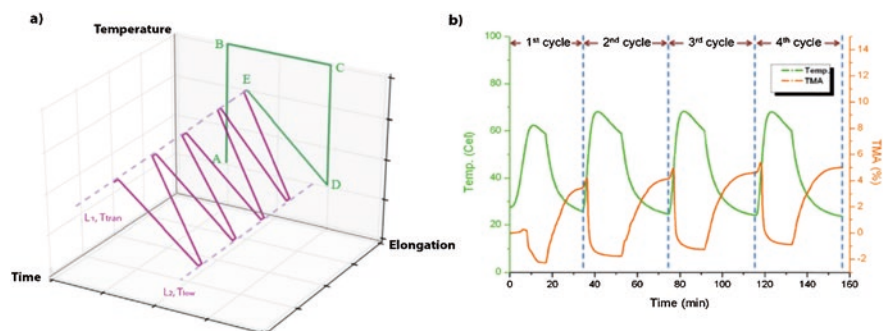

Fig. 5.30 (**a**) A diagrammatic sketch of thermomechanical training of 2W-SMP. The green path (A-E) is related to programming of 2W-SMPs and the purple path verifies the 2W-SME. (**b**) Cyclic behavior and TMA analysis of 2W-SMP based on the temperature variation [66]

conventional polymer with two separated transition temperatures. At first, the polymer is heated to T_1 which is above the two transition temperatures (T_{trans1}, T_{trans2}) and is deformed under external stress. And then the deformed sample is cooled to a temperature T_2, which is between T_{trans1} and T_{trans2}. At temperature T_2, the polymer segments with T_{trans1} are frozen, and the related entropy and elastic energy are stored in the frozen phase. After unloading the external stress, the first temporary shape ($\varepsilon1$) is obtained. In the second step, the first temporary shape is further deformed by external force, resulting in a further reduced entropy; thus, the recovery force is formed. Cooling to temperature T_0 is below both two transition temperatures. At temperature T_0, the mobility of all polymer segments is frozen. Then, the second temporary shape ($\varepsilon2$) is obtained after unloading the external force. When the sample is heated from T_0 to T_2, the movement of chain segment with T_{trans2} is reactivated; thus, the sample returns to the first temporary shape ($\varepsilon1$), which is attributed to the releasing of the stored elastic energy. At last, the sample continues to be heated to T_1, and it recovers to its original shape because the remaining stored elastic energy is released.

As mentioned above, the polymer with a broad transition range can produce TSME. For instance, the polymer shows a broad glass transition range, which can be found in two or more separated Tgs. Xie and coworkers reported an amorphous polyurethane network with one broad Tg showing good TSME, as shown in Fig. 5.32 [76]. The samples in original rectangular shape are changed into the "SMP" letters shape by plastic deformation. Then, the permanent shapes are deformed to temporary shape of "SIC" and "ZJU" according to the triple-shape
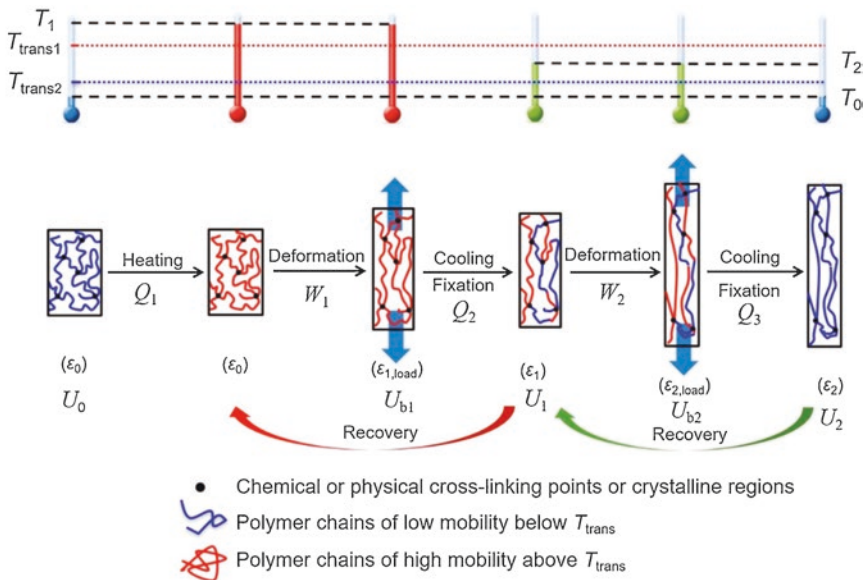

Fig. 5.31 Schematic illustration and the molecular mechanism of a conventional TSME [75]

memory programming procedures. During the shape recovery process, the samples are first heated to 80 °C to recover to shape "SIC" and then further heated to 120 °C to recover to the permanent shape "SMP." In addition, miscible polymer blends and random copolymers with broad Tg can satisfy the basic requirement of TSME [77–79]. Except for the broad glass transition, a broad melting transition range may also make polymers with TSME [80]. There is no specific value for the width of Tg to make the polymer have TSME. However, a wider range of Tg can give the polymer better shape retention and recovery ratios. Furthermore, a wider range of Tg can achieve more recoverable shapes, which means the polymer can achieve four or even multiple shape memory effects.

5.3.2.4 Multiple Shape Memory Effect

Multiple shape memory effect can be regarded as the extension of TSME, that is to say, the polymer can present more than three shape changes during recovery process. According to different mechanisms, multiple SME can be divided into two categories: one is internal multiple SME and the other is external multiple SME [55]. For intrinsic multiple SME, the molecular requirement is almost the same as the traditional two-way SME (2W-SME). The netpoint structure is responsible for maintaining the permanent shape, and the switching phase is responsible for fixing temporary shape and shape recovery. In multiple SME, the netpoint structure plays the same role, while the difference lies in the switching phase, which should be more versatile. For example, the polymer with TSME requires two transition temperatures undergoing two-step programming. It can be concluded that the TSME is an extension of the two-way SME. Similarly, TSME can be further extended to quadruple-SME (even multiple SME) following the same principle. This means that the number of temporary shapes that can be fixed depends on the number of different transitions in the polymer structure. Theoretically, to achieve multiple SME, the polymer must have multiple distinct transitions, which is a challenge for polymer synthesis. The more transitions are needed, the more difficult the polymer synthesis will be.

In 2010, Xie first exploited multiple SME in commercial polyelectrolyte (PFSA) with a broad Tg [81]. The PFSA possesses a broad glass transition temperature range from 55 °C to 130 °C. They found that a quadruple-SME could be obtained with this single transition when the polymer was deformed and fixed to temporary shapes at different temperatures. This type of multiple SME is quite different from the abovementioned type, which needs different distinct transitions. For PFSA, multiple temporary shapes can recover at the recovery temperatures which are corresponding to the deformed temperatures. PFSA can memorize three temporary shapes through the same programming procedure. Multiple SME of PFSA originates from its broad glass transition. This broad glass transition can be regarded as a collection of numerous small transition units. For shape memory effect, these transitions can be viewed as independent memory units based on deformation temperatures, resulting in multiple shape memory effect. Chen and his collaborator

Plasticity performance:
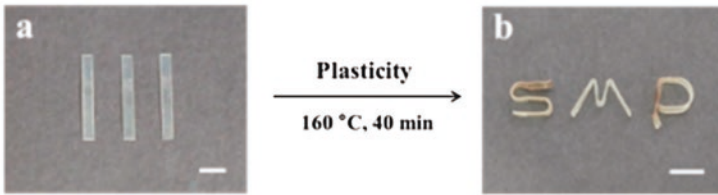
Triple-shape memory performance:
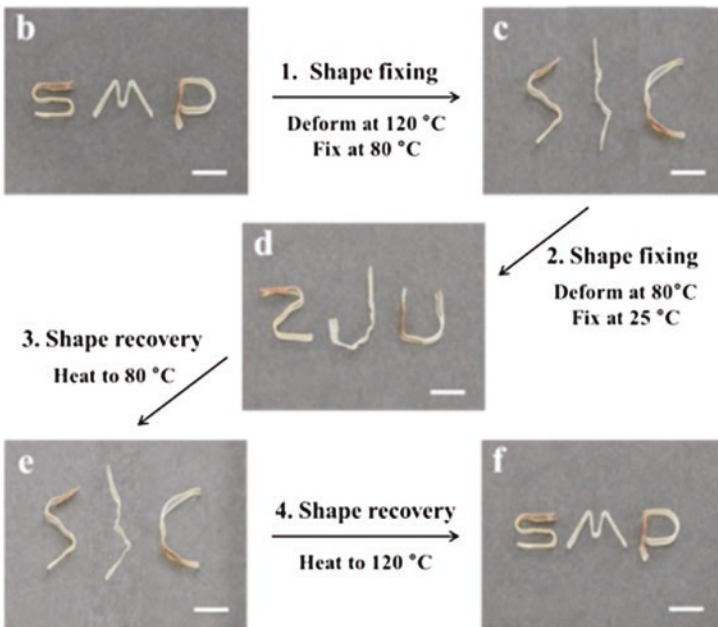
Fig. 5.32 The photos of PU with TSME. (**a**) Original shapes. (**b**) Permanent shapes. (**c**) First temporary shape "SIC." (**d**) Second temporary shapes "ZJU." (**e**) First recovery to temporary shape "SIC." (**f**) Recovery to permanent shapes "SMP." Scale bar: 8 mm [76]

fabricated a chemically cross-linked zwitterionic shape memory polyurethanes (CZPU), which possesses a broad glass transition, as shown in Fig. 5.33a. The broad glass transition makes CZPUs prohibit multiple SME, and the shape fixation and recovery of CZPU are excellent due to the chemical cross-linking structure, as displayed in Fig. 5.33b [82].

5.3.3 Other Stimuli-Responsive SMPs

At present, shape recovery process can be driven by several other stimulus methods, which can be divided into two categories. One is inherent stimuli-induced SMPs (without temperature change) such as solvent, pH, metal ion, etc. The other is indirect heating-responsive SMPs (with temperature change), such as near-infrared light, electricity, magnetic field, microwave, etc. Although body heat is the most important actuation method for biomedical applications, the indirect heating method has many advantages due to more convenient and noncontact remote control, which can broaden its application in medical devices.

5.3.3.1   Electric-Induced Shape Memory Polymers

Electrical stimulation is very convenient and allows for a local stimulus response in some cases. The use of electrical stimulation shape has produced a great increase in the applications of shape memory polymers. In general, nano-fillers are good conductive materials, such as conducting polymers, carbon black (CB), carbon nanotubes (CNTs), and carbon nanofibers, and when they are introduced into the substrate of the polymer, electric resistivity is significantly reduced and joule heating occurred and enabled electrically conductive SMPs [83, 84]. In 2004, Goo reported that the electrically stimulated shape memory polymers where CB and CNTs act as nano-fillers endow the nanocomposites good electrical conductivity [85]. When the content of CB is 30 wt%, the electrical conductivity of the nanocomposite can reach to 10 S/cm. However, the high loading content of CB significantly decreases the shape memory effect of the nanocomposites. To overcome this shortcoming, Sh and workers [86] prepared nanocomposites comprising of PU/PLA and surface-modified carbon nanotubes by melt mixing. The resistivity of nanocomposites filled with 10 wt% of CNTs decreased to about 66.7% in comparison to pristine CNT-filled polymer blend composites. Low concentrations of CNTs (~2 wt%) can significantly enhance mechanical and thermal properties. In SME experiment,
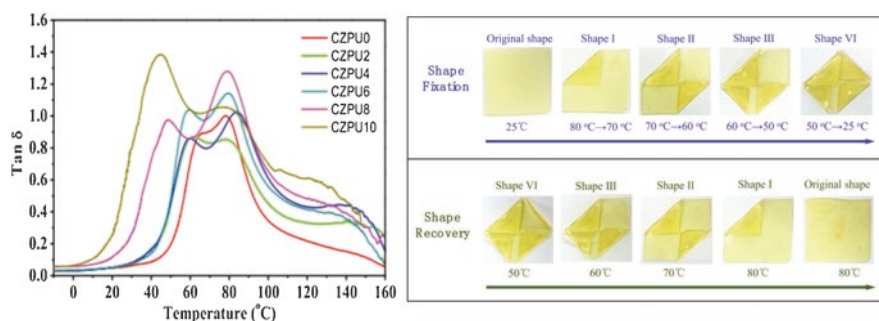

Fig. 5.33 (**a**) DMA curves of CZPUs, (**b**) digital images of quintuple shape memory behaviors of CZPU10

nanocomposites filled with CNTS can have a complete recovery of its original structure by applying electrical impulses of 15 s and 40s. Leng [87] groups used carbon nanofiber (CNF) and boron nitride (BN) nanopaper self-assembly to provide conductive doping and then coated on the surface of SMP, which can achieved 96.7% shape recovery in 80 s at 4.8 V. CNF and BN in nanopaper have a synergistic effect on the electrically induced shape recovery behavior of SMP nanocomposites. They further reported epoxy-based shape memory (ER) composites doped with reduced graphene oxide paper (rGOP) [88]. Compared to most previous reports, rGOP/ER composites can recover to its permanent shape within 5 s at 6 V which is more energy saving and more fast speed than the previously reported data, as shown in Fig. 5.34. Fu et al. reported shape memory polymer nancomposites of PPC/PLA/MWCNTS, which reached a shape recovery ratio of 97% within 30 s at 30 V [89]. Bai prepared CB-doped PLA/TUP/CB SMP, which show improved mechanical properties and outstanding electrical conductivities with low filler content. The nanocomposites exhibited a good electro-induced shape memory effect, which could recover to their original shape within 80 s at 30 V [90].

5.3.3.2 Magnetic-Induced Shape Memory Polymers

Generally speaking, magnetic-induced shape memory effect can be obtained by adding magnetic nanoparticles to the SMPs. Under alternating magnetic field, the magnetic fillers play the role of transferring electromagnetic energy to thermal energy, which leads to shape recovery at noncontact mode. This initiation method has potential applications in biomedical fields. The typical fillers used to realize the magnetic-induced SME contains iron(III) oxide particles, ferromagnetic particles, NdFeB particles, and nickel powders [91]. Iron oxide (Fe_3O_4) nanoparticles become the most commonly used addition filler due to their high magnetism and good biocompatibility.

To realize excellent magnetic-induced SME, uniform distribution of fillers in the SMP matrix is required. For instance, Fe_3O_4 nanoparticles were surface-modified
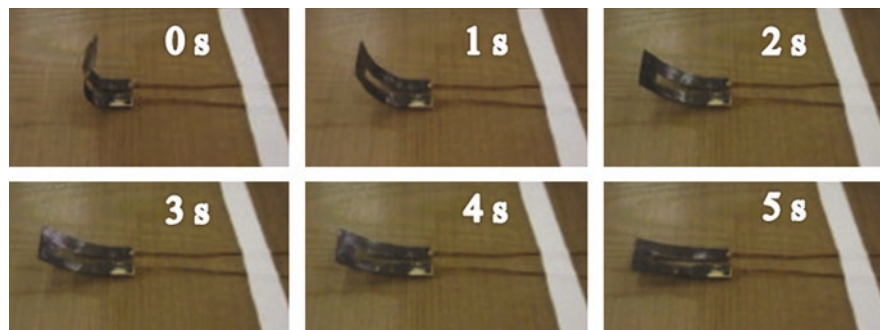
Fig. 5.34 Shape recovery process photo of RGOP/ER under applied 6 V Dc [88]

using PEG-10000 and then were dispersed in the PDLLA polymer matrix at different compositions. The SMP composites exhibited improved mechanical properties and magnetic-induced SME under alternating magnetic field, as shown in Fig. 5.35. The shape recovery ratio is up to 98% and affected by the entanglements of molecular chains and the nanoparticles' content [92]. Bai et al. explored a one-pot synthesis of norbornene-capped Fe_3O_4 nanoparticles, and then the particles copolymerized with norbornene through ring-opening polymerization to fabricate SMP composites. The Fe_3O_4 nanoparticles dispersed very well in the polymer matrix [93]. In this system, the Fe_3O_4 nanoparticles act as not only the cross-links of molecular chains but also the inductive heating elements.

Although magnetic-induced SME has many advantages in biomedical application, there are still some challenges for clinical application. Above all, the frequency of the magnetic field should be within safe range of clinical application. Moreover, heat is generated to raise the temperature under an alternating magnetic field, which should also be within the safe range of the human body to avoid harm to human tissues. Further research is needed to develop more suitable structures of magnetic-induced SMP, so that it can be used in practice.

5.3.3.3   Light-Induced Shape Memory Polymers

Light, the fastest growing renewable source, has proven to be the low loss, easy access, and environment friendly source of energy. In some special areas, light can be used to perform precise regulation and conversion of remote targets. Therefore, light-response SMP has been developed rapidly in recent years. Generally, there are

Fig. 5.35 Photographs showing shape recovery process of PDLLA/Fe_3O_4 nanocomposites at a weight ratio of 2:1 in a magnetic field taken by digital camera [58]

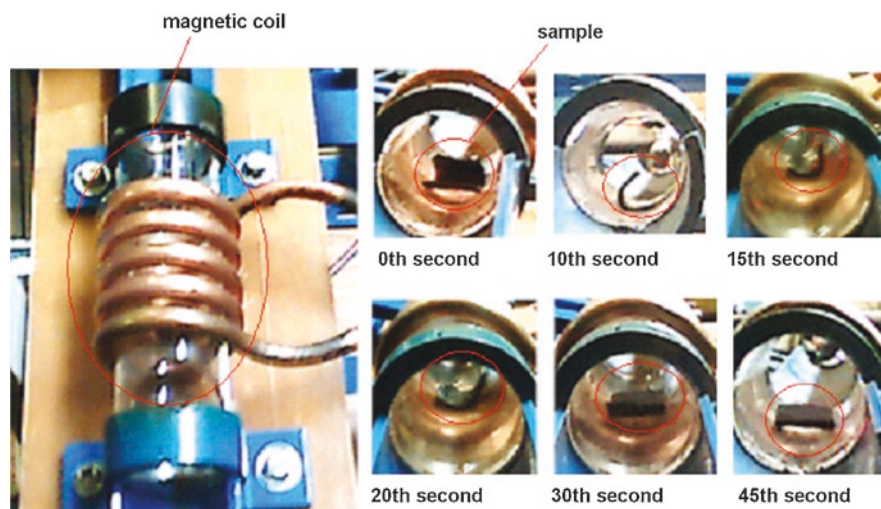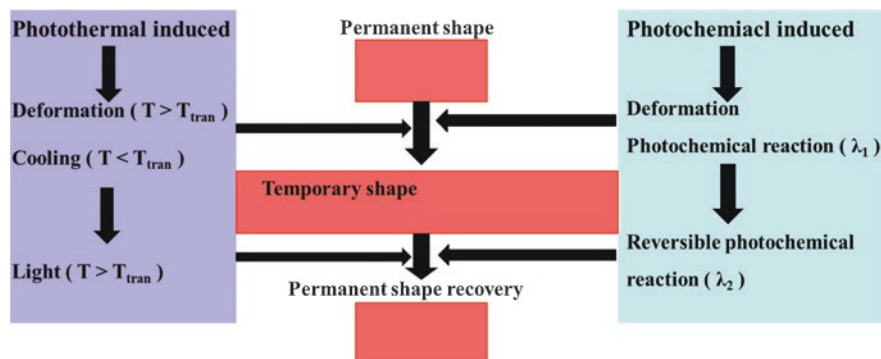| Photothermal induced | Permanent shape | Photochemiacl induced |
Deformation (T > T_tran)		Deformation
Cooling (T < T_tran)	Temporary shape	Photochemical reaction (λ₁)
Light (T > T_tran)	Permanent shape recovery	Reversible photochemical reaction (λ₂)

Fig. 5.36 Schematic illustration of light-triggered shape memory polymers based on either the photothermal effect or photochemical reactions

two recognized mechanisms for shape memory polymers. The first mechanism is photothermal-induced SMP as shown in Fig. 5.36. The polymers were heated to $T > T_{tran}$ and the temporary shape is obtained, and then T was reduced to Ttran to freeze the polymer chains. When the polymers were irradiated by UV–visible–near-infrared (NIR) light, they absorb the NIR and convert it into heat energy, which is transferred to the polymers through the photothermal conversion property. As a result, the temperature on the surface of the polymers rises, and the shape of the polymer is stimulated to recover. The second mechanism based on the photochemical reaction has a different principle. First of all, under the excitation of a specific wavelength $\lambda 1$, the polymer will undergo a light-induced cross-linking reaction, which will temporarily denature the polymer's shape. After that, under the excitation of a specific wavelength $\lambda 2$, the polymer can undergo a reversible photochemical reaction, resulting in shape recovery.

Light-response SMP according to the formation mechanism can be divided into two categories. One category is incorporation of photothermal media into SMP, such as conductive polymers, carbon materials, and metal nanoparticles [94–96]. Yin and coworkers reported a light-triggered SMP that is a nanocomposite material based on thermoplastic polyurethane (TPU), poly(ε-caprolactone) (PCL), and polydopamine (PDA ~1–3 wt%) by simple solution blending. PDA nanospheres acting as photothermal fillers can absorb NIR light which is converted into heat and then transferred to the polymer substrate to activate the recovery of the permanent shape [97]. The authors showed that NIR light-triggered shape recovery ratio of 100% could be observed with a composite material containing 3 wt% of PDA. In the same way as PDA, graphene oxide (GO) is a derivative of graphene which can also be used as nano-fillers for the photothermal-activated shape memory effect. Yu et al. investigated this by dispersing GO and azobenzene in PU. GO as photothermal fillers exhibited a light-responsive shape memory effect when the composites were irradiated by UV and NIR light [98]. Li formulated PU, epoxy, and epoxy-functionalized graphene oxide (DGEBA-f-GO) nanocomposites. The mechanical properties of the nanocomposite with 2 wt% of DGEBA-f-GO are 88.70% higher

than those of pure PU. Moreover, the temperature of the nanocomposite increased rapidly to 77.7 °C in 5 s due to the excellent photothermal conversion effect of GO, which quickly drive the material for shape recovery, and the shape recovery ratio is 98% [99]. Another type of nano-fillers with photothermal ability for SMP is gold nanoparticles. Gold nanoparticles can efficiently convert optical energy to heat. Williams studied two shape memory epoxy systems doped with dispersed spherical gold nanoparticles [100]. Firstly, Au NPs are stabilized with poly(ethylene oxide) (Au@PEO) and dodecyl chains (Au@DD), and Au NPs then can be uniformly dispersed in epoxy matrix. With the used low concentration of Au@PEO (0.01 wt% as metallic gold) and Au@DD (0.04 wt% as metallic gold) and an NIR (532 nm) intensity of 2 W/cm2, a bended bar (1.4 mm thickness) can recover its initial shape in a few seconds. In another report, Wang selected gold nanoparticles as nano-fillers to prepare the PCL/Au-rGO composites. Gold nanoparticles not only significantly enhanced the recovery stress but also have great potential in light energy harvesting and remote-controlled actuators as shown in Fig. 5.37 [101].

Other category is using photochemical reactions to realize the fixation of the temporary shape and the recovery of the permanent shape. The most typical example is a report on nature in 2005. Lendlein [48] chose cinnamic acid (CA) and cinnamylidene acetic acid (CAA) as photoresponsive switches to prepare two amorphous polymers. One is CA-modified cross-linked methacrylic acid and the other is CAA-terminated star-poly(ethylene glycol) interpenetrated into a cross-linked poly(n-butyl acrylate). CA and CAA groups undergo photoinduced cross-linking cycloaddition reaction at a certain UV wavelength ($\lambda > 260$ nm) and then a fixed temporary shape without cooling the polymer temperature. The permanent shape can be recovered, and when the polymers were exposed to UV light ($\lambda < 260$ nm), shape recovery process occurred for both moieties.
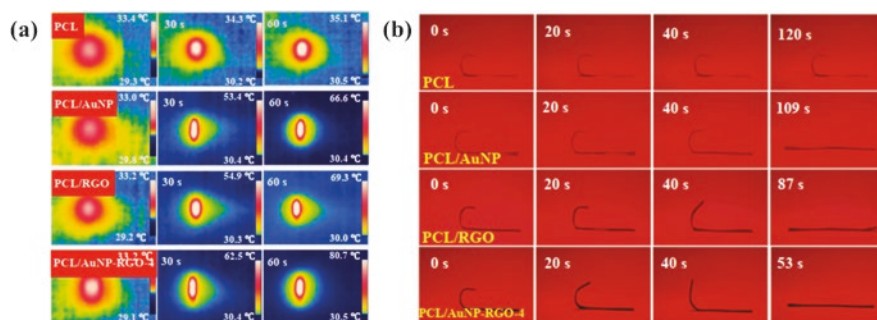

Fig. 5.37 (**a**) Infrared thermal imaging photographs showing the surface temperature changes of the samples with increasing time irradiated by 808 nm laser. (**b**) Digital photographs showing the shape recovery behavior of PCL composites under NIR light irradiation [101]

5.3.3.4 Water-/Solvent-Induced Shape Memory Polymers

Water-/solvent-induced SMPs were first reported in 2005 by Huang [102]. Since then, many SMPS with glass transition as switching transition have been found to possess such shape memory effect. The mechanism can be considered as the plasticizing effect of water or solvent on SMPs, which leads to an increase of the flexibility of macromolecules. Even if a small amount of water is added, the glass transition temperature of the SMPs may decrease. When the glass transition temperature drops close to the ambient temperature, the water-induced shape memory effect will be realized. For example, Huang and coworkers found that the glass transition temperature of the polyurethane SMP decreases obviously from 36 °C to 0 °C, when the fraction of moisture in weight increase from 0 to 4.5%.

At present, one of the effective methods to obtain water-induced SME is to introduce hydrophilic or water-soluble substances into SMPs. Cellulose (fiber, microcrystalline) is hydrophobic substance which is commonly used as filler to fabricate water-induced SMPs. Zhou et al. [103] prepared water-induced shape memory composites composed of microcrystalline cellulose (MCC) and poly(d,l-lactide) (PDLLA) using solution casting method. They found that the PDLLA/MCC composite shows excellent shape memory effect in water at 37 °C when the MCC content is 35%, as shown in Fig. 5.38.

Recently, water-induced SMPs are attracting more and more attention [104–107]. Water-induced SMEs open a new way for further applications of SMPs, especially in biomedical applications because the shape recovery can occur in the body fluid.

5.3.4 Clinical Applications of Shape Memory Polymers

Nowadays, SMP materials are emerging rapidly due to their superior properties. The developing multi-stimulative methods have widen the usage of SMP in various biomedical applications. These materials can be used in sutures, stents, tissue engineering, drug delivery, and other biomedical applications, which can solve the key problems of minimally invasive surgery. Meanwhile, relatively complex mechanical deformation operations can be performed automatically rather than manually by surgeons.

5.3.4.1 Applications in Endovascular Tissue Engineering

Vascular stent is a kind of tubular stent which can reopen the occluded and narrow vessels and restore the smooth flow of blood. At present, metals can be applied in the manufacture of stents as the main skeleton, but due to their high rigidity, they cannot be applied to winding blood vessels. Compared with metal bracket, the improvement of flexibility and compliance of SMP can solve this problem.
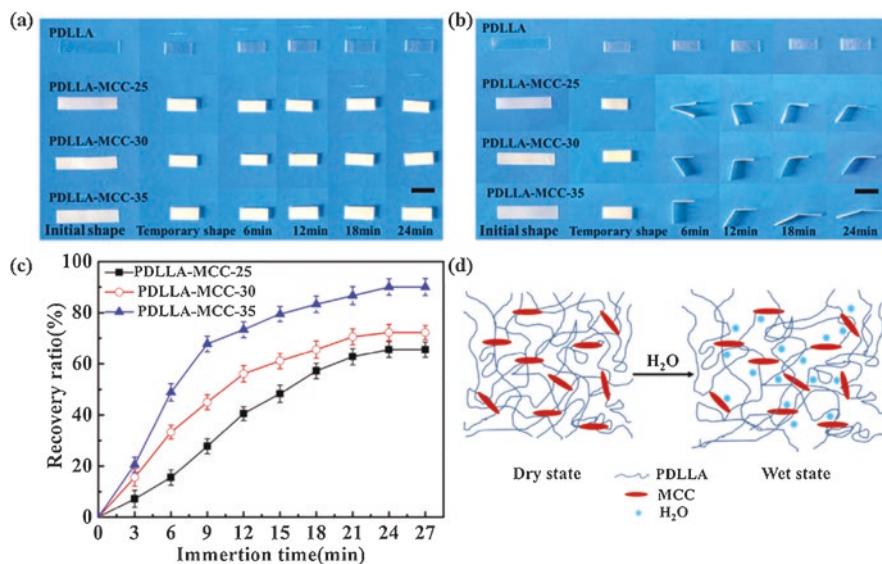
Fig. 5.38 (**a**) The photos show the shape memory effect of the pure PDLLA and PDLLA/MCC composites (**a**) in the dry state at 37 °C, (**b**) in the wet state at 37 °C, (**c**) shape recovery ratio as a function of time for the PDLLA/MCC composites in the wet state at 37 °C, (**d**) water-induced shape-memory mechanism of the PDLLA/MCC composites. Scale bars is 10 mm [103]

The incorporation of time dimension into 3D printing to form 4D printing has significant application prospects in artificial organs or tissues. Leng et al. [108] proposed two types of 4D printed shape memory stents with a remarkable shape recovery ratio and a negative Poisson's ratio structure. The experimental data manifested that the narrow blood vessel was dilated within 5 s. Huang and coworkers [109] obtained a water-induced programmable shape memory polymer device which is a promising candidate for minimally invasive surgery. It is a SMP film consisting of polyurethane, which can be folded into a preset shape and then transported to a designated position through a catheter and trigger shape recovery by absorbing body fluid. Sun et al. [110] reported a stent that was fabricated on the basis of the triple SMP, which held function of prompt retraction. Taking into account various unpredictable factors during the operation, the immediate removal of the stent makes the surgical operation more flexible and fault-tolerant. The block copolymer PCTBV-25 with thermal switching as rapid self-expandable stent was fabricated by Liang et al., as presented in Fig. 5.39 [111]. It consists of two parts: hyperbranched three-arm PCL and microbial polyester PHBV. Venkatraman et al. [112] developed a kind of Bi-layered SMP with elastic memory. It alleviated the elastic recoil that often occurs during the balloon expansion of polymeric stents. Through finite element analysis, Yu et al. [113] found that the shape memory polyurethane (SMPU) braided stent showed a gradual expansion (unfolded) characteristic with increasing body temperature, preventing sudden overpressure in the blood vessel wall during the process of blood vessel deployment.

Stroke is a grievous disease, which is attributed to blood clots clogged in blood vessels like stones. Thus, blood flow is interrupted, which prevents oxygen from being transported to the brain, causing the limbs to be useless. At present, the only approved treatment for acute ischemic stroke is intravenous injection of recombinant tissue plasminogen activator (tPA). The effectiveness of tPA restricts the time window of revascularization to 3 h after the onset of symptoms. Therefore, after 3 h, tPA is ineffective in dissolving blood clots. The endovascular device with shape memory function may be a promising tool for the treatment of ischemic stroke without the need for infusion of thrombolytic drugs. Maitland et al. [114] introduced that one way to treat ischemic stroke is through mechanical removal of the blood clots using a novel micro-actuator device. This characteristic polyurethane-based material can maintain a stable secondary shape and will return to its primal shape after controlled heating. The device is composed of an injection-molded SMP microactuator, which can be turned into a coil shape by optical heating, so as to grab blood clots from blood vessels and restore blood flow. In addition, they also made an umbrella device. The folded umbrella was pushed pass the thrombus, enabled to expand with a laser pulse of 0.25 W for 5 s, and triumphantly captured the thrombus.

Aneurysm is a balloon-like swelling of an artery wall. The swollen blood vessel wall becomes thin and easily ruptured, which is life-threatening. Transcatheter arterial embolization (TAE) is generally regarded as an efficacious way to treat aneurysm. TAE with metal microcoils is tended to recanalization as is known to all. They have low filling ratio, and it cannot be stacked tightly in the blood vessel because of their extreme rigidity. In the up-to-date research, SMP was proposed for the treatment of aneurysms. Zhang et al. [115] reported a radiopaque body temperature-induced shape memory (SM) hydrogel with high hardness. This gel network contains the dipole–dipole interaction of polyacrylonitrile/hydrogen bond physical interaction of polyacrylamide and chemical cross-linking of a long flexible PEG-3kDMA. The team gave gel X-ray imaging capabilities by direct $BaSO_4$

Fig. 5.39 Shape recovery of scaffold in water bath at 37 °C [111]
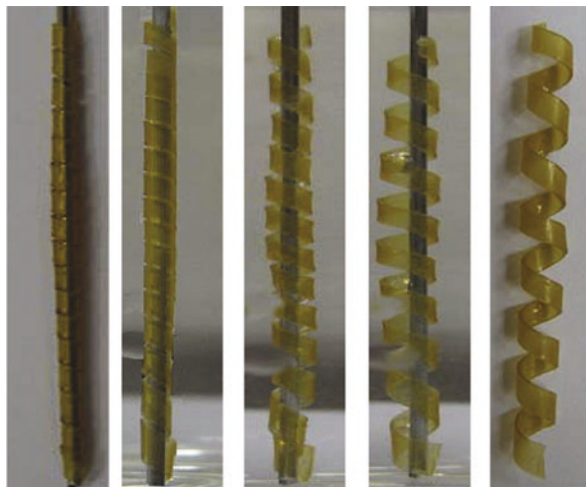
precipitation. In order to explore the effect of in vivo embolization, the team successfully reversed the method of pre-forming the gel with imaging function into a microcoil, which was heated and straightened and fixed at a low temperature into a straight strip. Under the protection of low-temperature physiological saline, it was delivered to the porcine renal artery through an interventional catheter. After contacting with "warm blood," the straight gel strip quickly transformed into a coil, and several coils were continuously delivered to successfully embolize the renal artery. The experiment findings reveal that 3 months after the operation, the kidneys showed obvious atrophy, indicating that there was no recanalization of the blood vessels. Kashyap et al. [116] reported a radiopaque and porous tungsten shape memory polyurethane (SMPU) with predominant shape holding and shape recovery of up to 100%. Moreover, the radiopacity and storage modulus of the SMPU are increased due to the addition of tungsten, which is expected to be used in the interventional treatment of aneurysms. But tungsten has a long-term genotoxicity in the physiological environment [117]. Oppositely, sulfate ($BaSO_4$) nanoparticles have antimicrobial characteristics [118], and HaP nanoparticles possess prominent hemostatic characteristics [119]. In subsequent research [120], the team proposed to add sulfate ($BaSO_4$) nanoparticles and hydroxyapatite (HaP) nanoparticles to the SMPU, which also makes the material to have radiopacity.

SMP foam is implanted into aneurysm after compaction. Because of the shape memory effect, aneurysm can be mildly filled during the expansion of aneurysm. Metcalfe et al. [121] proposed that cold hibernated elastic memory (CHEM) polyurethane-based foam was used for the treatment of carotid aneurysm as presented in Fig. 5.40. The results showed that the angiography score was good at 3 weeks. Neointima grew thicker on the foam of the neck of the aneurysm, and foam properties facilitate in the growth of cells during the formation of neointima. However, in some special cases, CHEM embolization of aneurysms may lead the blood to resume flowing smoothly, because the existing formula does not allow the cavity of the treated aneurysm to be completely filled. Small et al. [122] obtained a neoteric device for the therapy of fusiform (non-necked) aneurysms. This device consists of two main parts: SMP scaffold and SMP embolic foam. The experimental phenomenon manifested that the embolic foam accomplished embolization of the aneurysm lumen, while the stent kept an open-flow lumen in the parent artery.

In addition, a series of aliphatic urethane-based SMP were proposed by Kunkel et al. [123] that have shown potential applications in the treatment of intracranial aneurysms such as endovascular embolization devices.

5.3.4.2 Applications in Tissue Engineering

The tissue-engineered bone is one of the predominant curative methods for craniomaxillofacial (CMF) bone defects. For critical-sized craniomaxillofacial bone defects, match bone defects with irregular borders are precisely considerable. In some current studies, SMPs obtain extensive attention for irregular bone defect disease. Their shape memory behavior enables them to be delivered in a compressed
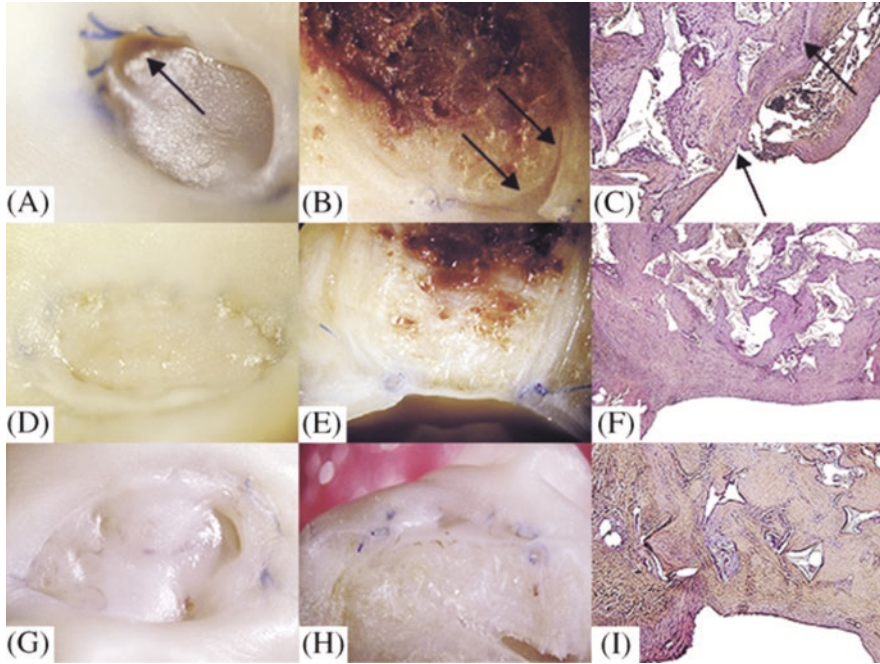
Fig. 5.40 Macroscopic and microscopic appearance of aneurysms embolized with CHEM sponges. (**a**), (**d**), (**g**) Macrophotographs of aneurysm necks "en face". (**b**), (**e**), (**h**) Macrophotographs of axial sections of aneurysms. (**c**), (**f**), (**i**) microscopic views of axial sections. [121]

form during minimally invasive surgery, and they can be restored to complex final shapes in vivo. Melissa A. Grunlan et al. [124] in their research used a SMP stent via photo-cross-linking of polycaprolactone. Good ductility allowed the cylindrical scaffold to be processed into various irregular shapes with the PCL heated. As the temperature decreased, the shape was fixed within the defect. In addition, it has osteoconductive and bioactive characteristics by coating bioactive polydopamine on the surface of the pore walls. The self-fitting actions of it were presented in Fig. 5.41.

In the repair of bone defects, it is a challenging task to implant large-volume porous scaffolds in a concise and reliable manner. Liu et al. [125] presented a porous smart nanocomposite scaffold. The scaffold was composed of chemically cross-linked poly(ε-caprolactone) (c-PCL) and hydroxyapatite nanoparticles. It not only has shape memory function but also controls the delivery of growth factors by coating the calcium alginate layer and BMP-2 on the surface of the pore wall. The diameter of the deformed pores after compression is 33 μm, and the diameter after restoration to the porous shape is 160 μm. The scaffold was implanted in the rabbit mandibular defect for bone tissue regeneration and ingrowth.

Richard M et al. [126] developed two special devices: expanded porous SMP grafts (acrylate-based) and compressed porous SMP sleeves (thermoplastic

Fig. 5.41 Self-fitting scaffold was processed into irregular shapes [124]

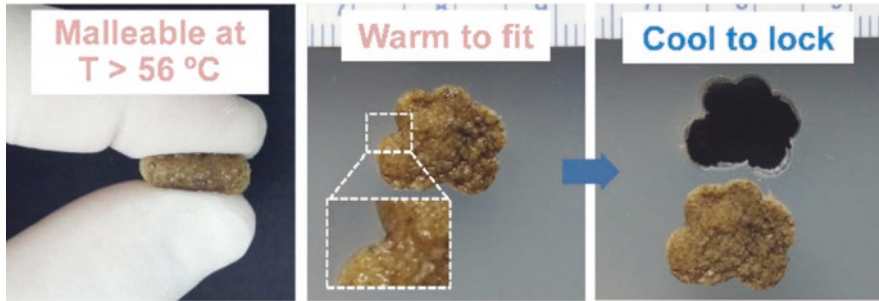polyurethane, TPU). In this research, they have exhibited the effect of intraoperative delivery and load bearing of SMP for transplanting and stabilizing complex bone defects. In addition, fibrous SMP scaffolds have been reported for use in bone regeneration. Bao et al. [127] reported an electrospun fibrous poly(D,L-lactide-co-trimethylene carbonate) scaffold. The scaffold availed the adhesion and proliferation of osteoblasts and facilitated mineral deposition.

Some unexpected disasters can cause damage to the peripheral nervous system. Nerve repair and regeneration are major clinical challenges. Many shortcomings of nerve autografts or artificial nerve elongation limit their therapeutic development. Therefore, the use of artificial nerve is an alternative treatment. A smart nerve conduit (SNC) is obtained by Chen et al. [128] that can markedly cut short the surgery procedure and attain predominant peripheral nerve regeneration (PNR) by automatic gradual lengthening. When the SMP nerve conduit is sutured with the tension-free end, the nerve damaged in body fluids exhibits self-healing behavior, which can induce the orientated growth of the cell and obtain a complete homologous nerve. Based on this material, a prototype of smart trigeminal conduit is developed and reveals prolonged gradual recovery function.

In Dan Kai et al.'s [129] research, using poly(PCL/PDMS urethane) as the skeleton, a battery of electrically conductive nanofibers with shape memory properties applied in smart four-dimensional (4D) stents for nerve tissue regeneration were fabricated by annexing different amounts of carbon black. Poly(PCL/PDMS urethane) shows superfast response and could be restored to its preset shape within 2 s [130]. The addition of carbon black does not affect its shape memory effect. This biomimetic nanofibrous scaffold displayed prominent electrical conductivity, remarkable shape memory properties, and good biocompatibility. It has been reported that the electrically conductive scaffold as an interchange venue for cell interaction can extend the length of neurites and facilitate the differentiation of neurons as presented in Fig. 5.42 [129]. Castillo-Cruz et al. [131] synthesized segmented polyurethanes based on L-lysine that would become promising candidate for large diameter vascular grafts where the arrangement of cells could be manipulated by their shape memory potential. And their team [132] proved that the

L-arginine-based SPUs promote the growth of endothelial cells which is suitable for small-diameter vascular grafts.

5.3.4.3   Applications in Surgical Suture

Traditional surgical sutures may give rise to wound infection and necrosis of surrounding tissue. Tiny forces can also leave scars during the stitching process. And some sutures need to be removed by a second operation. Langer et al. [133] developed a group of biodegradable shape memory polymer suture made by oligo(ε-caprolactone) diol (OCL). When the temperature rises to normal body temperature, it shrinks to tighten the wound. Especially, its degradable function avoids removing surgical sutures after surgery. Based on FDM printing, SMPs can be programmed in the gradient mode of the expected function during the manufacturing process, and M. Bodaghi et al. [134] proposed a new method to fabricate adaptive metamaterials. It is experimentally shown that the activation of the adaptive metamaterial triggers the shape to recover so that the two cloths are tightly connected. Using ethyl cellulose (EC) and polycaprolactone (PCL) as raw materials, a shape memory polymer with decent mechanical strength was prepared by Wang et al. [135]. The tensile modulus ranged from 104.9 to 373.4 MPa. The tensile strength varied from 155.4 to
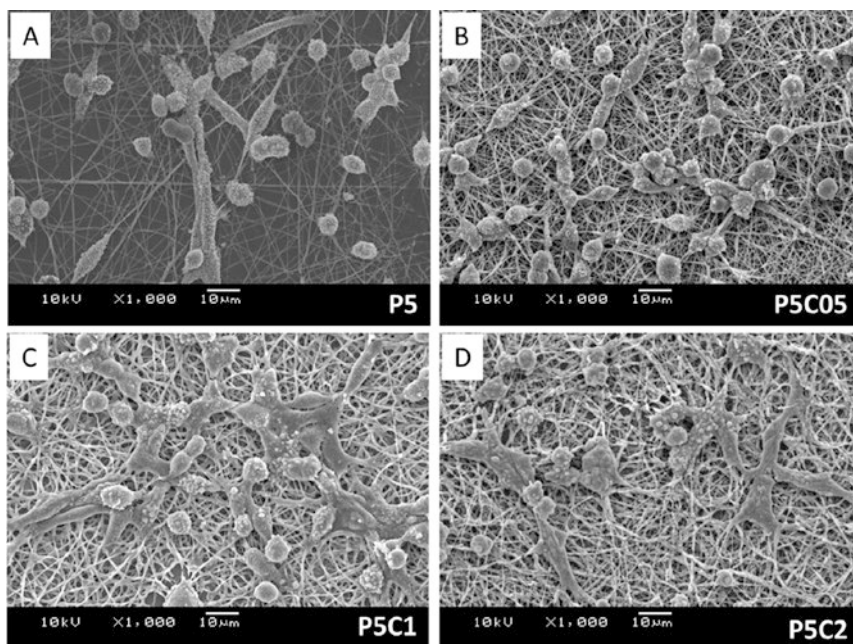
Fig. 5.42 Morphology of PC12 cells on electrospun, extending neurites to connect with the neighbour cell on different nanofibers with carbon black coded as (**a**) P5 (**b**) P5C05 (**c**) P5C1 (**d**) P5C2 [129]
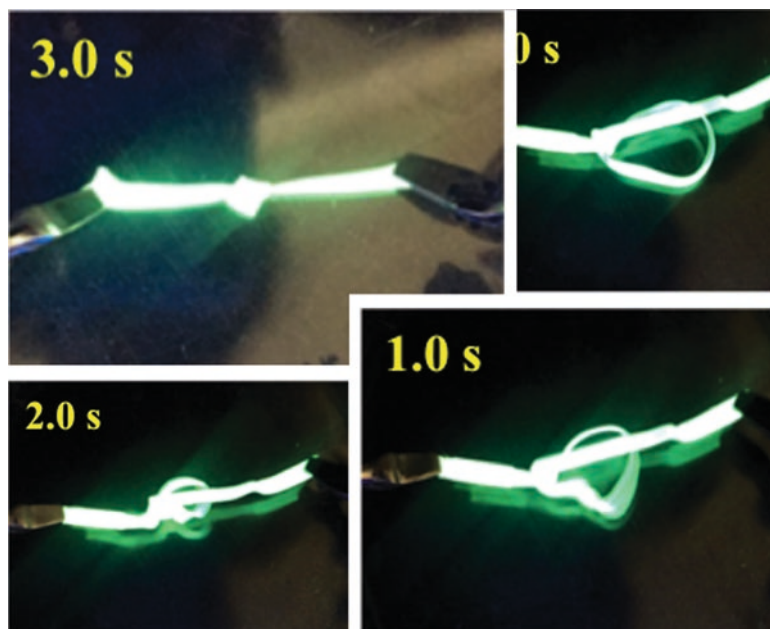
Fig. 5.43 Illustration of shape recovery process of 30%PU/PCL blend in a hot water bath [136]

323.6 MPa. The elongation at break was more than 621%. This biological friendly SMP is expected to be a hottest candidate for surgical sutures. Gong et al. [136] designed a biocompatible SMP composed of polyurethane (PU) and polycaprolactone (PCL) to be applied in smart suture applications. When the proportion of PU reached 30%, the polymer possessed the best shape memory effect and self-knotted in a hot water bath as presented in Fig. 5.43. In addition, some research developed a group of hardblock-free multiblock thermoplastic polyurethanes (TPUs) consisting of poly(ε-caprolactone) (PCL) and poly(ethylene glycol) (PEG) which are also the candidates for surgical sutures [51, 137].

5.3.4.4 Applications in Pharmaceutical Controlled Release System

The purpose of controlled drug release system is to regulate the speed, position, and dosage of drug release to suit the requirements of specific therapeutic applications. Lendlein et al. [138] applied a kind of biodegradable SMP based on the copolyester urethane network to drug delivery system. After the drugs were implanted in the surface of the SMP, the incorporated drugs form drug particles which were wrapped completely by the deformation of SMP. After the drug delivery system enters the body, by manipulating the shape recovery speed, the drug can appear in a specific position with a controllable speed and dose. The operation is fundamental of drug delivery system as presented in Fig. 5.44.

Drug-eluting stents have proven to be an excellent percutaneous strategy for patients with coronary disease [139]. Sung et al. [140] reported on a biodegradable sirolimus-eluting SMP stent that inhibits the formation of neointima, made from chitosan-based strips fixed by an epoxy compound. This SMP stent can operate the controlled release of sirolimus in a sustained manner and may be used to treat in-stent restenosis due to neointimal hyperplasia. Monika et al. [141] proposed a ter-polymer with shape memory property consisting of L-lactide, glycolide, and trimethylene carbonate (TMC) as drug-free matrix for a long-term paclitaxel delivery. Yan et al. [142] proposed a hydrogel complex with ultrahigh porosities (>95%) and decent water-sensitive shape memory property that can be used to control insulin delivery. The shape memory properties of this hydrogel composed of chitosan (CHIT) and agarose (Agar) are erasable and pH-dependent that can be altered by attached pH cues.

In addition to the above effects, controlled release preparations can also restrain drug degradation, alleviate side effects, or increase patient compliance with treatment. Moreover, self-anchoring implant rods [143] for a sustained drug release and different SMP storage systems for rapid stimuli-induced drug release have been proposed.

5.3.4.5   Applications in Hemostatic Agent

Rapid and effective hemostasis is an essential basic function for wound dressings. The use of compression bandages or gauze is the current conventional method of hemostasis treatment, but it is often ineffective for irregularly shaped and deep wounds. In addition, preventing bacterial infections is also an indispensable indicator of optimal wound dressings. Landsman et al. [144] designed a kind of fresh hydrogel-coated SMP foam with shape memory effect, hemostatic ability, and excellent antibacterial properties as a wound dressing. It consists of two parts: (1) polyurethane SMP foams for volume filling and rapid hemostasis and (2) iodine-doped (PEG-PVP) hydrogels for fluid uptake and bactericidal action. Compared with traditional wound dressings, this new material can absorb more liquid and has marvelous antibacterial ability. Liu et al. [145] reported on robust 3D porous
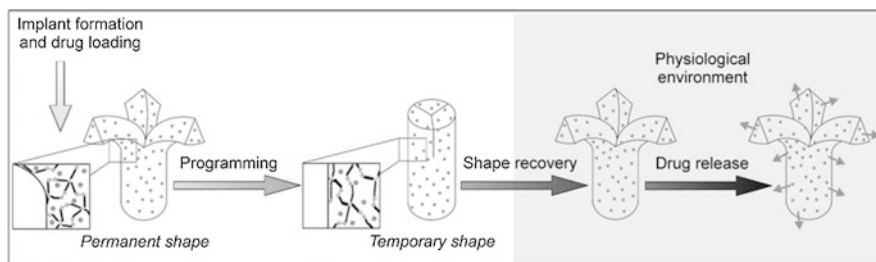
Fig. 5.44 Operating principle shape memory polymer drug-loaded devices [138]
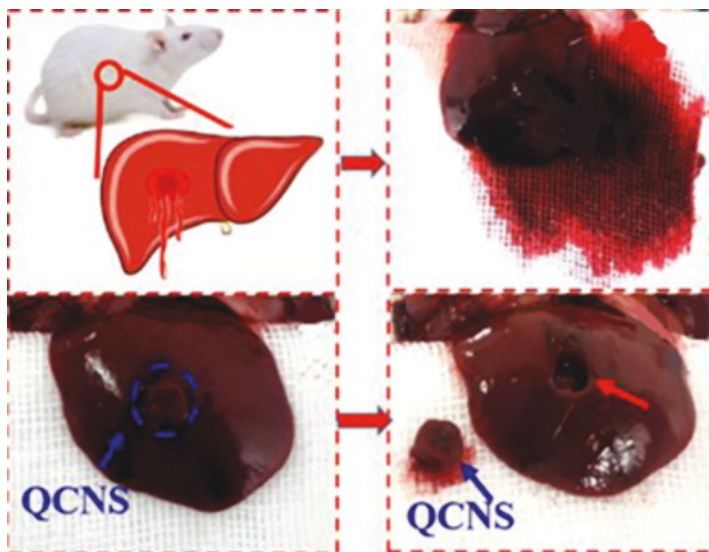
Fig. 5.45 Using the wound on rat liver as non-compressible wound model

sponges synthesized by chitin that had two blades: antibacterial and hemostatic. Ultrafast water/blood-triggered shape recovery performance (less than 1 s) allowed it to promptly expand to fill wounds when it touched blood. The results show that the multifunctional sponge is ideal for hemostatic dressings on incompressible wounds as presented in Fig. 5.45. Tan et al. [146] reported that the treatment of the blend of chitosan, gelatin and shape memory polyurethane (SMPU) with silver nitrate could impart SMP with antibacterial properties and further develop its potential in wound dressing.

5.3.4.6 Other Biomedical Applications

In addition to medical applications with several described examples of potential SMP medical devices as discussed above, other reports cover applications in several different parts of the body; e.g., Yakacki et al. [147] designed a shape memory polymer network customized by photopolymerization that can be used for soft tissue fixation in anterior cruciate ligament tear. Moreover, two bioinspired tracheal scaffolds are manufactured through 4D printing of magnetic-triggered shape memory PLA/Fe_3O_4 composite by Zhao et al. [148]

High intraocular pressure is mainly caused by the high pressure of aqueous humor on the eyeball. The aqueous humor is produced in the ciliary body, passes through the aqueous humor circulation path, and eventually returns to the vein. If the circulation of the aqueous humor is blocked, it can cause high intraocular pressure. The problem of blocked aqueous circulation can be ameliorated with implants.

Various SMP implants have been developed to reduce intraocular pressure [149]. The implant can open up a new path for circulation inside (stents) or ameliorate the blocked physiological channel and its surrounding tissues. Epiphora is a typical manifestation of nasolacrimal duct occlusion [150]. Park et al. [151] developed a shape memory polymer (SMP) with self-expanding elasticity that can be used as an alternative to traditional silicone intubation (stenting) to physically open drainage channels and ensure liquid flow. SMPs (94%PCL, 6%PGMA) possess more predominant drainage ability and decent resistance to bacterial infection. Due to the recovery from a thinner threadlike shape to a custom-fit tube, the difficulty of surgical operation would be reduced. SMPs may be used as a substitute for traditional materials to remedy dental malocclusion. Compared with traditional dental braces, SMP possesses more aesthetic attraction. It is easy to mount and tailor shape. Lightweight and more comfy experience is also its highlight. Jung et al. [152] developed a shape memory polyurethane with high shape retention, and shape recovery can achieve tooth alignment in orthodontic treatment. In the in vitro model, the shape of the SMP wire gradually recovers as the temperature rises, and the powerful restoring force causes the irregular teeth to be calibrated. Thermomechanical testing indicated that the stable shape recovery force can keep the SMP wire in a fixed shape for up to 3 months. Furthermore, this new type of orthodontic appliance looked more aesthetically appealing.

The stomach of obese people is usually oversize, which causes them to want to eat more food to fill it. In a report [153], a SMP device was mentioned, which can enter the stomach in a small volume and expand in the stomach after stimulation, thereby reducing the volume of the stomach. Decreased stomach volume can lead to faster satiety during ingestion. And this device can be mechanically fixed in the stomach without affecting the food passing through the pylorus. Bowel anastomosis is a common surgical operation to connect two stumps to restore the opening of the lumen patency. The entero-entero anastomosis (EEA) ring stapler with only one nail line is prone to local inflammation and fluid leakage [154]. Paonessa et al. [155] proposed a bioartificial hydrogel with a ring memory shape composed of polyvinyl alcohol (PVA) and gelatin. The addition of acetylsalicylic acid reduces postoperative inflammation. Fisher et al. [156] designed a radially expanding shape memory polymer based on the acrylic SMP to elongate the intestine and grow a new tissue.

Arteriovenous fistula is a commonly used vascular access for maintenance hemodialysis patients. Under the effect of the needle flow, arteriovenous fistula suffered a high level of hemodynamic pressure, which may lead to occlusion of vascular access. Ortega et al. [157] studied the application of SMP on renal dialysis needle. This SMP adapter is installed on the needle, and when it is thermally stimulated, it will expand into a tubular shape with a larger cross-sectional area than the needle tube. This morphology can adjust the hydrodynamics of the needle flow to lessen the hemodynamic stress of the arteriovenous graft. The blood flow has changed after installing the SMP adapter as presented in Fig. 5.46. In a few literature reports [158], SMP has also been proposed to apply to female contraception. SMP implants are inserted into the fallopian tubes temporarily or permanently through catheters during routine procedures such as transcervical surgery. The implant will expand
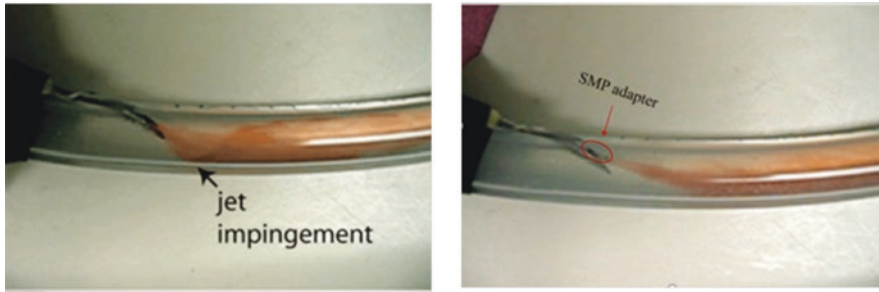
Fig. 5.46 Changes in blood flow before and after deploying SMP adapter

into a specific shape within the body temperature range, forming a blockage in the fallopian tube, and the ovum in the fallopian cannot successfully migrate to the uterus.

In addition to the abovementioned applications, many unanticipated SMPs are being developed and used in the biomedical field. Proteins and DNA are essentially polymers. A recently reported document proposes an artificial nail, which is fabricated of translucent keratin [159]. Studies have found that this material has a marvelous thermo-/moisture-inductive shape memory effect. These devices made of autologous protein/DNA may alleviate immunological rejection caused by allogeneic implants. The shape memory role in protein/DNA will have many potential applications waiting to be discovered. Miao et al. [160] designed a 4D printing ink with shape memory effect. Polymerized soybean oil-epoxidized acrylate as a kind of bio-link for 4D printed scaffold has extremely high shape recovery rate and hMSC adhesion and proliferation.

Although SMPs have many medical applications as described above, they still have challenges in sterilization, biodegradation, and cytotoxicity for further biomedical applications. For example, some existing sterilization methods may change their physical or chemical structures, as a result of changing their thermal-induced shape memory effect. In addition, from the perspective of medical application, all the selected shape memory polymers have good biocompatibility; however, inflammatory reaction due to implanted devices is widespread. All the abovementioned problems need to be solved by further research work.

5.4 Concluding Remarks

SMMs had been successfully used in the field of biomedical application. The future trends in shape memory biomaterials (SMBs) can be expected at different aspects: (1) research and development of new kinds of SMBs, (2) combination of the functional properties of SMBs with the structural properties of other biomaterials to

form shape memory hybrids (SMHs) or shape memory composites (SMCs), and (3) new technology applied to shape SMBs.

5.4.1   R&D on New SMBs

As is mentioned above, the TiNi SMAs have been fabricated into medical devices and widely used in the clinic, including dentistry, orthopedics, vascular surgery, and so on. However, after implantation of the traditional TiNi SMAs, these devices would exist in the human body for a lifetime unless it is removed by the second surgery. This problem could be solved by biodegradable SMAs, which could degrade as implantation time prolongs. It is generally accepted that the biodegradable metals include Mg-, Fe-, and Zn-based alloys with proper alloying elements. It should be noticed that a new kind of Mg-based shape memory alloys has been reported [161] in 2016, and the alloy system is Mg–Sc alloy system. Both thermal- and stress-induced martensites have been verified in this work. The β-type Mg–Sc alloy with a body-centered cubic (bcc) structure could transform into martensite phase with orthorhombic structure. The martensite phase was detected by XRD analysis of Mg-19.2 at.% Sc when the ambient temperature decreased from 20 °C to −190 °C, whereas no phase transformation was detected on Mg-20.5 at.% Sc at the same experimental condition. This phenomenon illustrated that the martensitic transformation-starting temperature, M_S, is strongly dependent on Sc content, which would increase with decreasing Sc content. The stress-induced martensitic transformation was verified by cyclic tensile test. It came out that the maximum superelasticity of Mg-20.5 at.% Sc alloy was 4.4%, which is obtained at −150 °C. By comparing the superelasticity and specific weight of the Mg–Sc alloys with other polycrystalline SMAs, it is found that the β-type Mg–Sc alloy system exhibits comparable superelasticity with β-type Ti alloys but much lower specific weight [161].

The above report on shape memory magnesium alloy makes the application of biodegradable SMAs promising. In order to evaluate the potential usage of such shape memory magnesium alloy in the clinic, Liu et al. [162] fabricated the Mg–Sc alloy with similar Sc content and carried out the in vitro and in vivo studies. It came out that β-phased Mg–Sc alloy exhibited excellent mechanical performance. The presence of Sc could effectively incorporate into the corrosion product and fill the corrosion pits. The degradation rate of β-phased Mg–Sc alloy is only 0.06 mm·y^{-1} in vivo, which would not lead to the continuous accumulation of Sc in animals' main organs. On the whole, it is believed that the orthopedics application of shape memory Mg–Sc alloy would be promising.

However, until now, the study on biodegradable SMAs is still scarce. There are still many problems needing to be solved. As for the reported Mg–Sc shape memory alloy, the martensitic transformation temperature is essential to be elevated to near-body temperature. Besides, because of the expensive price of Sc, it would be better to reduce Sc content or find alternative elements without deteriorating its shape

memory effect. Last but not least, it is necessary to explore the SME of other biodegradable alloy systems.

5.4.2 Shape Memory Hybrids (SMHs)

At present, shape memory hybrid (SMH) is emerging as a new member of the SMM family. The concept of SMH is featured by its easy accessibility so that even a non-professional person can design and fabricate his/her own SMM to meet the particular requirements of an application. Fundamentally speaking, in terms of working mechanism, SMHs share many similarities as that of SMPs, in which there are at least two components (segments or domains), one is always elastic (elastic component, including chain entanglement in some glassy SMPs) and the other is able to significantly alter its stiffness (transition component, may be also called switch segments sometimes) if the right stimulus is applied. The key difference between SMH and shape memory composite is that the materials available for both components' selection of SMH are virtually without any limit. In other words, as for SMH, none of the components is required to have the SME as an individual. In shape memory composite, which is fabricated by the addition of the conductive particles, magnetic particles, and laser dyes into SMM, at least one conventional SMM (most likely, either SMA or SMP) is included. In fact, the components' types of SMH are various, including not only organics and inorganics but also metals. All of them could be selected as the elastic component or as the transition component. Therefore, the design of SMH is highly flexible for desired performance. With the components' ratio altered, both the structure and properties of the hybrid would change correspondingly, which further makes the acquisition of SMH with desired performance easier. The performance of SMH could be superior to all of its single components.

Ma et al. [163] prepared the EVA/PLA blends with different composition ratios. Due to the sufficient supply of PVAc group by EVA for the interaction with PLA, the elongation and impact properties of PLA/EVA improved 28 times and 2 times, respectively. Based on the above advantages, more and more attention has been paid on the development of SMH. Since some SMHs are of good biocompatibility and some of their components have already been applied in biomedical field, the biomedical application of SMHs is promising.

Xiao et al. [164] prepared the PNB/PLA hybrids with different composition ratios and evaluate its shape memory effect. Both dual and triple shape memory effects have been verified. It came out that the PNB/PLA hybrids with the proportion of 80/20 exhibit excellent shape recovery and shape fixed rates. The entangled macromolecular chains in PNB act as the physical cross-linking points and limit its movement and therefore promote the shape recovery properties of the hybrids. Because of the good biocompatibility and biodegradability of PLA, it is believed that the shape memory PNB/PLA hybrid is promising in the clinic.

Espinha et al. [165] reported a shape memory cellulose-based photonic reflector which could be a good candidate for biomedical application. The hybrid was

fabricated by impregnating and embedding colored cellulose nanocrystal (CNC) films with hydroxyl-dominant poly(dodecanediol-co-citrate) (PDDC-HD). The film's structural coloration and its high mechanical cohesion are achieved by the CNCs, while the SME is attributed to the PDDC-HD. In order to evaluate the shape recovery process of the CNC/PDDC-HD hybrid, the sample was preheated above the melting transition temperature (~30 °C), rolled up and maintained for a while. Then, the sample was cooled to room temperature, and its shape was mechanically held until complete solidification. Afterward, by applying a mild heat stress, the sample's shape recovered, regardless of gravity bias, as is presented in Fig. 5.47 [165]. Since such functional and responsive material could perform from room to body temperature, it is hopeful to be used in biomedical field.

As is mentioned in Sect. 5.3.3.4, when hydrophilic or water-soluble substances are introduced into SMPs, the shape memory effect might be triggered by water/solvent. It is found that the SMHs feasible for biomedical application also possess similar effect. Fan et al. [166] proposed two approaches for the fabrication of water-responsive SMHs, the temporary shape of which are respectively achieved by the recrystallization of the inclusion material inside the deformed porous matrix as well as deforming after heating the hybrid to the inclusion's melting temperature and cooling back. The polymer sponge/cupric sulfate pentahydrate hybrid was fabricated according to the former approach. And according to the latter one, the silicone/sodium acetate trihydrate hybrid was prepared. This kind of hybrid could recover to its original shape within different time, which is dependent on water temperature. Since the inclusion materials' type of the water-responsive SMH is versatile, its applications are extensive. Taken its application of retractable eluting
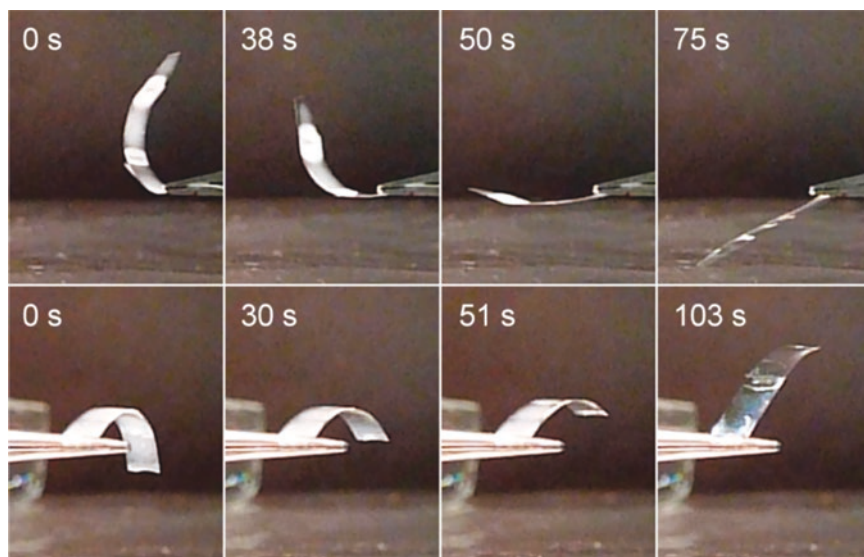

Fig. 5.47 Shape recovery process of CNC/PDDC-HD hybrid at different times. The top row is in favor of gravity while the bottom one is against it [165]

shape memory stent as an example, medicines could act as the inclusion of SMH and be released gradually. The shape memory stent could shrink to a small size for easy removal.

Furthermore, in order to avoid the overheating problem of SMM in biomedical field, Wang et al. [167] proposed a cooling-/water-responsive SMH whose transition temperature is near-body temperature. The hybrid could recover to its original shape within shorter times at lower water temperature. It is made of a plastic sponge filled with Poloxamer 407 (P407). The former acts as the elastic component, while the latter acts as the transition component. As for biomedical application, the plastic sponge could be replaced by other biocompatible and biodegradable materials (e.g., PLA). Such SMH could be adopted as suture with adjustable stiffness, the delivery system via minimally invasive surgery, and so on.

Although SMPs have many medical applications as mentioned above, there are still challenges in sterilization, biodegradability, and cytotoxicity for further applications. For example, some sterilization methods may change their physical or chemical structures, as a result of changing the thermal-induced SME. The degradation of materials will have an impact on SME, and how to match the degradation of materials with the use situation is still a research direction. In addition, from the perspective of medical application, all the selected materials have good biocompatibility; however, there are inflammatory responses induced by implantable devices. All the problems need to be solved by further research work.

5.4.3 New Technology Applied to SMBs

5.4.3.1 4D Printing

Additive manufacturing (AM), that is, three-dimensional (3D) printing, has become a popular method for complex objects manufacturing by joining or layering materials. In virtue of computer-aided design (CAD), the 3D objects could be printed. On the basis of 3D printing, the concept of 4D printing was put forward, which highlights time as the fourth dimension. The 4D printing objects could be regarded as the stimuli-responsive 3D printed objects. Under specific external environmental stimuli (e.g., heat, humidity, pH, light, etc.), its physical properties and performance would change with time. Especially, smart materials with SME are able to recover their shapes with environmental changes. Among them, SMPs are concerned as good candidates for 4D printing. The methods for 4D printing SMPs mainly include fused deposition modeling (FDM), stereolithography apparatus (SLA), PolyJet, and direct-writing (DW). By 4D printing, the structure of SMPs could be designed according to the specific application. Besides, the objects could be pre-deformed to their minimum volume and recover back to their original shapes when they are in service. These advantages promote the biomedical application of 4D printing SMPs, which has been introduced in detail in Sect. 5.3.4. However, there are still some limitations. With regard to biocompatibility, the FDA-approved materials (e.g.,

PCL, PLA, etc.) with high resolution cannot be printed by SLA process. On the other hand, the glass transition temperatures of 4D printing objects are always too high for the human body, which could be improved by copolymerization for changing the length of cross-link polymers.

5.4.3.2 Thin Film

As is known to us, nitinol has been successfully used in many endovascular applications. However, when nitinol is used with synthetic graft materials (e.g., expanded ePTFE, Dacron polyester), it is relatively bulky and is difficult to deliver in many trauma situations. TiNi SMA thin film is a new material which could help solve this problem.

Until now, by sputter deposition method, the high-quality nitinol thin film could be successfully fabricated. The compositional ratio and uniformity of nickel and titanium through its thickness could be controlled properly. After proper heat treatment, the nitinol thin film could possess similar desired properties (e.g., superelasticity, SE) as bulk nitinol. The microstructure of thin films would influence both transformation temperature and thin film stress, which are two primary parameters for the determination of shape memory effect and superelasticity. As for the microstructure, the grain size of the crystals and the types and distributions of precipitates are two primary aspects. By suitable compositional control and post-heat treatment, the desired properties of films could be achieved.

To improve the biocompatibility of TiNi SMA thin film, new surface treatment method has been developed. It came out that TiNi SMA thin film demonstrated an excellent hemocompatibility according to the in vitro and in vivo tests when compared with the commercially available endovascular graft materials (e.g., ePTFE, Dacron polyester) [168]. Therefore, TiNi SMA thin film has been further developed into novel endovascular devices, including stent grafts, neurovascular flow diverters, heart valves, etc. [168]. Here, a hyperelastic thin film nitinol-covered flow diverter for the treatment of cerebral aneurysms is taken as an example [168]. Figure 5.48a and b shows two hyperelastic thin film nitinol with different axis lengths, porosities, and pore densities. Figure 5.48 (c) shows the flow diverter device with TiNi SMA thin film covering around the commercially available stent [168].
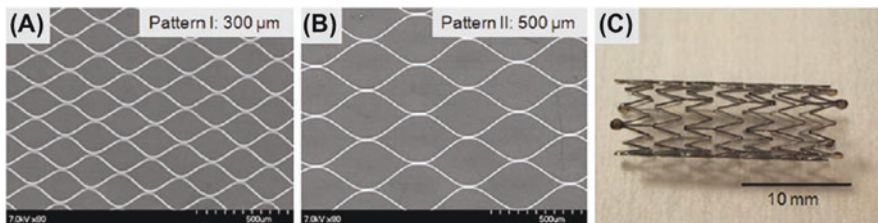

Fig. 5.48 Hyperelastic thin film nitinol with different axis length (**a**) 300 μm, (**b**) 500 μm, and (**c**) a model of hyperelastic thin film nitinol-covered stent [168]

Chun et al. [169] implanted the TiNi SMA thin film flow diverter into swine and verified its efficacy and safety. The occlusion time of aneurysm sac for the devices was only 10 to 68 min, while the control bare metal stent was up to 4 h. According to the histopathology results, healthy neointima layer covered the aneurysmal neck, and its sac was resorbed by the surrounding tissue.

5.4.4   Shape Memory Ceramics

On the whole, the shape memory biomaterials, mainly including shape memory alloys, shape memory polymers, shape memory composites, and shape memory hybrids, as well as their clinical application have been reviewed in this chapter. However, as for shape memory ceramics, including viscoelastic, martensitic, ferroelectric, and ferromagnetic shape memory ceramics, the biomedical application of them is still lacking. Although a few bioinert ceramics used in dentistry and orthopedics [170], that is, zirconia (ZrO_2) and alumina (Al_2O_3), belong to shape memory ceramics, their shape recovery characteristics have not been employed in biomedical field since their recoverable strains are very limited (< 0.1%). We do expect that there will be a breakthrough in the coming future.

References

1. Jani JM, Leary M, Subic A, Gibson MA. A review of shape memory alloy research, applications and opportunities. Mater Des. 2014;56:1078–113.
2. Xie T. Recent advances in polymer shape memory. Polymer. 2011;52:4985–5000.
3. Nemat-Nasser S, Guo W. Superelastic and cyclic response of NiTi SMA at various strain rates and temperatures. Mech Mater. 2006;38:463–74.
4. Jiang F, Liu Y, Yang H, Li L, Zheng Y. Effect of ageing treatment on the deformation behavior of Ti–50.9 at.% Ni. Acta Mater. 2009;57:4773–81.
5. Zheng Y, Jiang F, Li L, Yang H, Liu Y. Effect of ageing treatment on the transformation behavior of Ti–50.9 at.% Ni alloy. Acta Mater. 2008;56:736–45.
6. Duerig T, Pelton A, Stöckel D. An overview of nitinol medical applications. Mater Sci Eng A. 1999;273:149–60.
7. Andreasen GF, Hilleman TB. An evaluation of 55 cobalt substituted Nitinol wire for use in orthodontics. J Am Dent Assoc. 1971;82:1373–5.
8. Torrisi L. The NiTi superelastic alloy application to the dentistry field. Biomed Mater Eng. 1999;9:39–47.
9. Peters OA, Azevedo Bahia MG, Pereira ESJ. Contemporary root canal preparation: innovations in biomechanics. Dent Clin N Am. 2017;61:37–58.
10. Cheung GS, Liu CS. A retrospective study of endodontic treatment outcome between nickel-titanium rotary and stainless steel hand filing techniques. J Endod. 2009;35:938–43.
11. Shah KC, Chao D, Wu BM, Jensen OT. Shape-memory retained complete arch guided implant treatment using nitinol (Smileloc) abutments. Oral Maxillofac Surg Clin North Am. 2019;31:427–35.
12. Shah KC, Linsley CS, Wu BM. Evaluation of a shape memory implant abutment system: An up to 6-month pilot clinical study. J Prosthet Dent. 2020;123:257–63.

13. Willmott H, Al-Wattar Z, Halewood C, Dunning M, Amis A. Evaluation of different shape-memory staple configurations against crossed screws for first metatarsophalangeal joint arthrodesis: a biomechanical study. Foot Ankle Surg. 2018;24:259–63.

14. Laravine J, Loubersac T, Gaisne E, Bellemère P. Evaluation of a shape memory staple (Qual®) in radial shortening osteotomy in Kienböck's disease: a retrospective study of 30 cases. Hand Surg Rehabil. 2019;38:141–9.

15. Schipper ON, Ellington JK. Nitinol compression staples in foot and ankle surgery. Orthop Clin North Am. 2019;50:391–9.

16. Bansiddhi A, Sargeant T, Stupp SI, Dunand DC. Porous NiTi for bone implants: a review. Acta Biomater. 2008;4:773–82.

17. Andani MT, Moghaddam NS, Haberland C, Dean D, Miller MJ, Elahinia M. Metals for bone implants. Part 1. Powder metallurgy and implant rendering. Acta Biomater. 2014;10:4058–70.

18. Bertheville B. Porous single-phase NiTi processed under Ca reducing vapor for use as a bone graft substitute. Biomaterials. 2006;27:1246–50.

19. Xu Y, Qi B, Fan X, Xu X, Lu S, Ding J. Four-corner arthrodesis concentrator of nickel-titanium memory alloy for carpal collapse: a report on 18 cases. J Hand Surg Am. 2012;37:2246–51.

20. Li H, Mao Y, Qu X, Zhao X, Dai K, Zhu Z. Nickel-titanium shape-memory sawtooth-arm embracing clamp for complex femoral revision hip arthroplasty. J Arthroplast. 2016;31:850–6.

21. Kraemer M, Mueller CW, Hermann M, Decker S, Springer A, Overmeyer L, Hurschler C, Pfeifer R. Design considerations for a novel shape-memory-plate osteosynthesis allowing for non-invasive alteration of bending stiffness. J Mech Behav Biomed Mater. 2017;75:558–66.

22. Patel SM, Li J, Parikh SA. Design and comparison of large vessel stents: Balloon expandable and self-expanding peripheral arterial stents. Interv Cardiol Clin. 2016;5:365–80.

23. Garcia L, Jaff MR, Metzger C, et al. Wire-interwoven nitinol stent outcome in the superficial femoral and proximal popliteal arteries: twelve-month results of the SUPERB trial. Circ Cardiovasc Interv. 2015;8:e000937.

24. Zhou XC, Yang F, Gong XY, Zhao M, Zheng YF, Sun ZL. New nitinol endovascular stent-graft system for abdominal aortic aneurysm with finite element analysis and experimental verification. Rare Metals. 2019;38:495–502.

25. Zhou X, Yang F, Gong X, Zhao M, Zheng Y, Sun Z. Development of new endovascular stent-graft system for type B thoracic aortic dissection with finite element analysis and experimental verification. J Mater Sci Technol. 2019;35:2682–92.

26. Irani S, Kozarek R. Esophageal stents: past, present, and future. Tech Gastrointest Endosc. 2010;12:178–90.

27. Vakil N, Morris AI, Marcon N, et al. A prospective, randomized, controlled trial of covered expandable metal stents in the palliation of malignant esophageal obstruction at the gastro-esophageal junction. Am J Gastroenterol. 2001;96:1791–6.

28. Tobis JM, Abudayyeh I. New devices and technology in interventional cardiology. J Cardiol. 2015;65:5–16.

29. Masura J, Gavora P, Podnar T. Long-term outcome of transcatheter secundum-type atrial septal defect closure using Amplatzer septal occluders. J Am Coll Cardiol. 2005;45:505–7.

30. Alkhouli M, Sievert H, Rihal CS. Device embolization in structural heart interventions: incidence, outcomes, and retrieval techniques. JACC Cardiovasc Interv. 2019;12:113–26.

31. Ahmed O, Sheikh S, Tran P, et al. Inferior vena cava filter evaluation and management for the diagnostic radiologist: a comprehensive review including inferior vena cava filter-related complications and PRESERVE trial filters. Can Assoc Radiol J. 2019;70:367–82.

32. Elahinia M, Moghaddam NS, Andani MT, Amerinatanzi A, Bimber BA, Hamilton RF. Fabrication of NiTi through additive manufacturing: a review. Prog Mater Sci. 2016;83:630–63.

33. Habijan T, Haberland C, Meier H, Frenzel J, Wittsiepe J, Wuwer C, Greulich C, Schildhauer T, Köller M. The biocompatibility of dense and porous nickel–titanium produced by selective laser melting. Mater Sci Eng C. 2013;33:419–26.

34. Zhang M, Yu Q, Liu Z, Zhang J, Tan G, Jiao D, Zhu W, Li S, Zhang Z, Yang R, Ritchie RO. 3D printed Mg-NiTi interpenetrating-phase composites with high strength, damping capacity, and energy absorption efficiency. Sci Adv. 2020;6:eaba5581.
35. Ramezannejad A, Xu W, Xiao W, Fox K, Liang D, Qian M. New insights into nickel-free superelastic titanium alloys for biomedical applications. Curr Opin Solid State Mater Sci. 2019;23:100783.
36. Liang C, Rogers CA, Malafeew E. Investigation of shape memory polymers and their hybrid composites. J Intell Mater Syst Struct. 1997;8:380–6.
37. Ware T, Simon D, Hearon K, Liu C, Shah S, Reeder J, et al. Three-dimensional flexible electronics enabled by shape memory polymer substrates for responsive neural interfaces. Macromol Mater Eng. 2012;297:1193–202.
38. Lu H, Yu K, Liu Y, Leng J. Sensing and actuating capabilities of a shape memory polymer composite integrated with hybrid filler. Smart Mater Struct. 2010;19:065014.
39. Gök MO, Bilir MZ, Gürcüm BH. Shape-memory applications in textile design. Procedia Soc Behav Sci. 2015;195:2160–9.
40. Hu ZL, Zhu Y, Huang HH, Lu J. Recent advances in shape–memory polymers: structure, mechanism, functionality, modeling and applications. Prog Polym Sci. 2012;37:1720–63.
41. Liu C, Qin H, Mather PT. Review of progress in shape-memory polymers. Chem. 2007;17:1543–58.
42. Ji FL, Hu JL, Li TC, Wong YW. Morphology and shape memory effect of segmented polyurethanes. Part I: with crystalline reversible phase. Polymer. 2007;48:5133–45.
43. Zhu Y, Hu J, Yeung K, Liu YQ, Liem H. Influence of ionic groups on the crystallization and melting behavior of segmented polyurethane ionomers. J Appl Polym Sci. 2006;100:4603–13.
44. Rousseau IA, Qin HH, Mather PT. Tailored phase transitions via mixed-mesogen liquid crystalline polymers with silicon-based spacers. Macromolecules. 2005;38:4103–13.
45. Ahn S-k, Deshmukh P, Kasi RM. Shape memory behavior of side-chain liquid crystalline polymer networks triggered by dual transition temperatures. Macromolecules. 2010;43:7330–40.
46. Lee KM, Wang DH, Koerner H, Vaia RA, Tan L-S, Angew TJW. Enhancement of photogenerated mechanical force in azobenzene functionalized polyimides. Chem Int Ed. 2012;51:4117–21.
47. Li J, Viveros JA, Wrue MH, Anthamatten M. Shape-memory effects in polymer networks containing reversibly associating side-groups. Adv Mater. 2007;19:2851–5.
48. Lendlein A, Jiang H, Jünger O, Langer R. Light-induced shape-memory polymers. Nature. 2005;434:879–82.
49. Wu LB, Jin CL, Sun XY. Synthesis, properties, and light-induced shape memory effect of multiblock polyesterurethanes containing biodegradable segments and pendant cinnamamide groups. Biomacromolecules. 2011;12:235–41.
50. Inomata K, Nakagawa K, Fukuda C, Nakada Y, Sugimoto H, Nakanishi E. Shape memory behavior of poly(methyl methacrylate)-graft-poly(ethylene glycol) copolymers. Polymer. 2010;51:793–8.
51. Gu X, Mather PT. Entanglement-based shape memory polyurethanes: synthesis and characterization. Polymer. 2012;53:5924–34.
52. Yang R, Chen L, Ruan C, Zhong H-Y, Wang Y-Z. Chain folding in main-chain liquid crystalline polyesters: from π–π stacking toward shape memory. J Mater Chem C. 2014;2:6155–64.
53. Petisco-Ferrero S, Fernández J, Fernández San Martín MM, Santamaría Ibarburu PA, Sarasua Oiz JR. The relevance of molecular weight in the design of amorphous biodegradable polymers with optimized shape memory effect. J Mech Behav Biomed Mater. 2016;61:541–53.
54. Navarro-Baena I, Sessini V, Dominici F, Torre L, Kenny JM, Peponi L. Design of biodegradable blends based on PLA and PCL: from morphological, thermal and mechanical studies to shape memory behavior. Polym Degrad Stab. 2016;132:97–108.
55. Zhao Q, Qi HJ, Xie T. Recent progress in shape memory polymer: new behavior, enabling materials, and mechanistic understanding. Prog Polym Sci. 2015;49-50:79–120.

56. Wong YS, Venkatraman SS. Recovery as a measure of oriented crystalline structure in poly(L-lactide) used as shape memory polymer. Acta Mater. 2010;58:49–58.
57. Thomsen DL, Keller P, Naciri J, Pink R, Jeon H, Shenoy D, et al. Liquid crystal elastomers with mechanical properties of a muscle. Macromolecules. 2002;34:5868–75.
58. Krause S, Zander F, Bergmann G, Brandt H, Wertmer H, Finkelmann H. Nematic main-chain elastomers: coupling and orientational behavior. C R Chim. 2009;12:85–104.
59. Broemmel F, Kramer D, Finkelmann H. Preparation of liquid crystalline elastomers. Adv Polym Sci. 2012;250:1–48.
60. Chung T, Romo-Uribe A, Mather PT. Two-way reversible shape memory in a semicrystalline network. Macromolecules. 2008;41:184–92.
61. Zhou J, Turner SA, Brosnan SM, Li Q, Carrillo JMY, Nykypanchuk D, et al. Shapeshifting: reversible shape memory in semicrystalline elastomers. Macromolecules. 2014;47:1768–76.
62. Li J, Rodgers WR, Xie T. Semi-crystalline two-way shape memory elastomer. Polymer. 2011;52:5320–5.
63. Tobushi H, et al. Two-way bending properties of shape memory composite with SMA and SMP. Materials. 2009;2:1180–92.
64. Ghosh P, Rao A, Srinivasa AR. Design of multi-state and smart-bias components using shape memory alloy and shape memory polymer composites. Mater Des. 2013;44:164–71.
65. Kang T-H, et al. Two-way actuation behavior of shape memory polymer/elastomer core/shell composites. Smart Mater Struct. 2012;21:035028.
66. Wu Y, Hu J, Han J, Zhu Y, Huang H, Li J, et al. Two-way shape memory polymer with "switch–spring" composition by interpenetrating polymer network. J Mater Chem A. 2014;2:18816–22.
67. Ratna D, Karger-Kocsis J. Shape memory polymer system of semi-interpenetrating network structure composed of crosslinked poly (methyl methacrylate) and poly (ethylene oxide). Polymer. 2011;52:1063–70.
68. Zare M, Prabhakaran MP, Parvin N, Ramakrishna S. Thermally-induced two-way shape memory polymers: mechanisms, structures, and applications. Chem Eng J. 2019;374:706–20.
69. Bellin I, Kelch S, Langer R, Lendlein A. Polymeric triple-shape materials. Proc Natl Acad Sci U S A. 2006;103:18043–180437.
70. Xiao LP, Wei M, Zhan MQ, Zhang JJ, Xie H, Deng XY, et al. Novel triple-shape PCU/PPDO interpenetrating polymer networks constructed by self-complementary quadruple hydrogen bonding and covalent bonding. Polym Chem. 2014;5:2231–41.
71. Wang L, Yang X, Chen H, Gong T, Li W, Yang G, et al. Design of triple-shape memory polyurethane with photo-cross-linking of cinnamon groups. ACS Appl Mater Interfaces. 2013;5:10520–8.
72. Chatani S, Wang C, Podgórski M, Bowman CN. Triple shape memory materials incorporating two distinct polymer networks formed by selective Thiol-Michael addition reactions. Macromolecules. 2014;47:4949–54.
73. Fu S, Zhang H, Zhao Y. Optically and thermally activated shape memory supramolecular liquid crystalline polymers. J Mater Chem C. 2016;4:4946–53.
74. Chen S, Yuan H, Chen S, Yang H, Ge Z, Zhuo H, et al. Development of supramolecular liquid-crystalline polyurethane complexes exhibiting triple-shape functionality using a one-step programming process. J Mater Chem A. 2014;2:10169–81.
75. Wang K, Jia Y-G, Zhao C, Zhu XX. Multiple and two-way reversible shape memory polymers: design strategies and applications. Prog Mater Sci. 2019;105:100572.
76. Zheng N, Hou J, Xu Y, Fang Z, Zou W, Zhao Q, et al. Catalyst-free thermoset polyurethane with permanent shape reconfigurability and highly tunable triple-shape memory performance. ACS Macro Lett. 2017;6:326–30.
77. Samuel C, Barrau S, Lefebvre J-M, Raquez J-M, Dubois P. Designing multiple-shape memory polymers with miscible polymer blends: evidence and origins of a triple-shape memory effect for miscible PLLA/PMMA blends. Macromolecules. 2014;47:6791–803.

78. Shao Y, Lavigueur C, Zhu XX. Multishape memory effect of norbornene-based copolymers with cholic acid pendant groups. Macromolecules. 2012;45:1924–30.
79. Li X, Pan Y, Zheng Z, Ding X. A facile and general approach to recoverable high-strain multishape shape memory polymers. Macromol Rapid Commun. 2018;39:1700613.
80. Yang X, Wang L, Wang W, Chen H, Yang G, Zhou S. Triple shape memory effect of star-shaped polyurethane. ACS Appl Mater Interfaces. 2014;6:6545–54.
81. Xie T. Tunable polymer multi-shape memory effect. Nature. 2010;464:267–70.
82. Zhou HT, Mei ZK, Chen H, Chen SJ. Chemically-crosslinked zwitterionic polyurethanes with excellent thermally-induced multi-shape memory effect and moisture-induced shape memory effect. Polymer. 2018;148:119–26.
83. Liu XF, Li H, Zeng QP, Zhang YY, Kang HM, Duan HN, Guo YP, Liu HZ. Electro-active shape memory composites enhanced by flexible carbon nanotube/graphene aerogels. J Mater Chem A. 2015;3:11641–9.
84. Xiao Y, Zhou S, Wang L, Gong T. Electro-active shape memory properties of poly(ε-caprolactone)/functionalized multiwalled carbon nanotube nanocomposite. ACS Appl Mater Interfaces. 2010;2:3506–14.
85. Cho JW, Kim JW, Jung YC, Goo NS. Electroactive shape-memory polyurethane composites incorporating carbon nanotubes. Macromol Rapid Commun. 2005;26:412–6.
86. Raja M, Ryu SH, Shanmugharaj AM. Thermal, mechanical and electroactive shape memory properties of polyurethane (PU)/poly (lactic acid) (PLA)/CNT nanocomposites. Eur Polym J. 2013;49:3492–500.
87. Lu HB, Huang WM, Leng JS. Functionally graded and self-assembled carbon nanofiber and boron nitride in nanopaper for electrical actuation of shape memory nanocomposites. Composites Part B. 2014;62:1–4.
88. Wang W, Liu D, Liu Y, Leng J, Bhattacharyya D. Electrical actuation properties of reduced graphene oxide paper/epoxy-based shape memory composites. Compos Sci Technol. 2015;106:20–4.
89. Qi X, Dong P, Liu Z, Liu T, Fu Q. Selective localization of multi-walled carbon nanotubes in bi-component biodegradable polyester blend for rapid electroactive shape memory performance. Compos Sci Technol. 2016;125:38–46.
90. Qi XD, Xiu H, Wei Y, Zhou Y, Guo Y, Huang R, Bai HW, Fu Q. Enhanced shape memory property of polylactide/thermoplastic poly(ether)urethane composites via carbon black self-networking induced co-continuous structure. Compos Sci Technol. 2017;139:8–16.
91. Zhang DW, Liu YJ, Leng JS. Magnetic field activation of thermoresponsive shape-memory polymer with embedded micron sized Ni powder. Adv Mater Res. 2010;123–125:995–8.
92. Zheng XT, Zhou SB, Xiao Y, Yu XZ, Li XH, Wu PZ. Shape memory effect of poly(d,l-lactide)/Fe3O4 nanocomposites by inductive heating of magnetite particles. Colloids Surf B: Biointerfaces. 2009;71:67–72.
93. Bai S, Zou H, Dietsch H, Simon YC, Weder C. Functional Iron oxide nanoparticles as reversible crosslinks for magnetically addressable shape-memory polymers. Macromol Chem Phys. 2014;215:398–404.
94. Du WN, Jin Y, Lai SQ, Shi LJ, Fan WH, Pan JZ. Near-infrared light triggered shape memory and self-healable polyurethane/functionalized graphene oxide composites containing diselenide bonds. Polymer. 2018;158:120–9.
95. Du W, Jin Y, Lai S, Shi L, Shen Y, Yang H. Multifunctional light-responsive graphene-based polyurethane composites with shape memory, self-healing, and flame retardancy properties. Composites Part A. 2020;128:105686.
96. Zhang HJ, Xia HS, Zhao Y. Light-controlled complex deformation and motion of shape-memory polymers using a temperature gradient. ACS Macro Lett. 2014;3:940–3.
97. Chen Y, Zhao X, Luo C, Shao Y, Yang MB, Yin B. A facile fabrication of shape memory polymer nanocomposites with fast light-response and self-healing performance. Composites Part A. 2020;135:105931.

98. Zhou L, Liu Q, Lv X, Gao L, Fang S, Yu H. Photoinduced triple shape memory polyurethane enabled by doping with azobenzene and GO. J Mater Chem C. 2016;4:9993–7.

99. Punetha VD, Ha Y-M, Kim Y-O, Jung YC, Cho JW. Interaction of photothermal graphene networks with polymer chains and laser-driven photo-actuation behavior of shape memory polyurethane/epoxy/epoxy-functionalized graphene oxide nanocomposites. Polymer. 2019;181:121791.

100. Leonardi AB, Puig J, Antonacci J, Arenas GF, Zucchi IA, Hoppe CE, Reven L, Zhu L, Toader V, Williams RJJ. Remote activation by green-light irradiation of shape memory epoxies containing gold nanoparticles. Eur Polym J. 2015;71:451–60.

101. Li ST, Jin XZ, Shao YW, Qi XD, Yang JH, Wang Y. Gold nanoparticle/reduced graphene oxide hybrids for fast light-actuated shape memory polymers with enhanced photothermal conversion and mechanical stiffness. Eur Polym J. 2019;116:302–10.

102. Huang WM, Yang B, An L, Li C, Chan YS. Water-driven programmable polyurethane shape memory polymer: demonstration and mechanism. Appl Phys Lett. 2005;86:114105.

103. Liu Y, Li Y, Chen HM, Yang G, Zheng XT, Zhou SB. Water-induced shape-memory poly(d,l-lactide)/microcrystalline cellulose composites. Carbohydr Polym. 2014;104:101–8.

104. Song LF, Li YQ, Xiong ZQ, Pan LL, Luo QY, Xu X, Lu SR. Water-induced shape memory effect of nanocellulose papers from sisal cellulose nanofibers with graphene oxide. Carbohydr Polym. 2018;179:110–7.

105. Liu Y, Li Y, Yang G, Zheng X, Zhou S. Multi-stimulus-responsive shape-memory polymer nanocomposite network cross-linked by cellulose nanocrystals. ACS Appl Mater Interfaces. 2015;7:4118–26.

106. Dagnon KL, Way AE, Carson SO, Silva J, Maia J, Rowan SJ. Controlling the rate of water-induced switching in mechanically dynamic cellulose nanocrystal composites. Macromolecules. 2013;46:8203–12.

107. Butchosa N, Zhou Q. Water redispersible cellulose nanofibrils adsorbed with carboxymethyl cellulose. Cellulose. 2014;21:4349–58.

108. Lin C, Zhang L, Liu Y, Liu L, Leng J. 4D printing of personalized shape memory polymer vascular stents with negative Poisson's ratio structure: a preliminary study. Sci China Technol Sci. 2020;63:578–88.

109. Huang WM, Yang B, Liu N, Phee SJ. Water-responsive programmable shape memory polymer devices. International Conference on Smart Materials and Nanotechnology in Engineering; 2007.

110. Sun L, Huang WM. Mechanisms of the multi-shape memory effect and temperature memory effect in shape memory polymers. Soft Matter. 2010;6

111. Xue L, Dai S, Li Z. Biodegradable shape-memory block co-polymers for fast self-expandable stents. Biomaterials. 2010;31:8132–40.

112. Venkatraman SS, Tan LP, Joso JF, Boey YC, Wang X. Biodegradable stents with elastic memory. Biomaterials. 2006;27:1573–8.

113. Kim JH, Kang TJ, Yu WR. Simulation of mechanical behavior of temperature-responsive braided stents made of shape memory polyurethanes. J Biomech. 2010;43:632–43.

114. Maitland DJ, Metzger MF, Schumann D, Lee A, Wilson TS. Photothermal properties of shape memory polymer micro-actuators for treating stroke. Lasers Surg Med. 2002;30:1–11.

115. Zhang Y, Gao H, Wang H, Xu Z, Chen X, Liu B, et al. Radiopaque highly stiff and tough shape memory hydrogel microcoils for permanent embolization of arteries. Adv Funct Mater. 2018;28

116. Kashyap D, Kishore Kumar P, Kanagaraj S. 4D printed porous radiopaque shape memory polyurethane for endovascular embolization. Addit Manuf. 2018;24:687–95.

117. Shah Idil A, Donaldson N. The use of tungsten as a chronically implanted material. J Neural Eng. 2018;15:021006.

118. Aninwene GE 2nd, Stout D, Yang Z, Webster TJ. Nano-BaSO4: a novel antimicrobial additive to pellethane. Int J Nanomedicine. 2013;8:1197–205.

119. Song L, Sun L, Jiang N, Gan Z. Structural control and hemostatic properties of porous micro-spheres fabricated by hydroxyapatite- graft -poly(DL-lactide) nanocomposites. Compos Sci Technol. 2016;134:234–41.
120. Kashyap D, Gaur SS, Kanagaraj S. Development of hybrid shape memory polyurethane composites for endovascular applications. Mater Today Commun. 2020;22
121. Metcalfe A, Desfaits A-C, Salazkin I, Yahia LH, Sokolowski WM, Raymond J. Cold hibernated elastic memory foams for endovascular interventions. Biomaterials. 2003;24:491–7.
122. Small W, Buckley PR, Wilson TS, Benett WJ, Hartman J, Saloner D, et al. Shape memory polymer stent with expandable foam: a new concept for endovascular embolization of fusiform aneurysms. IEEE Trans Biomed Eng. 2007;54:1157–60.
123. Kunkel R, Laurence D, Wang J, Robinson D, Scherrer J, Wu Y, et al. Synthesis and characterization of bio-compatible shape memory polymers with potential applications to endovascular embolization of intracranial aneurysms. J Mech Behav Biomed Mater. 2018;88:422–30.
124. Zhang D, George OJ, Petersen KM, Jimenez-Vergara AC, Hahn MS, Grunlan MA. A bioactive "self-fitting" shape memory polymer scaffold with potential to treat cranio-maxillo facial bone defects. Acta Biomater. 2014;10:4597–605.
125. Liu X, Zhao K, Gong T, Song J, Bao C, Luo E, et al. Delivery of growth factors using a smart porous nanocomposite scaffold to repair a mandibular bone defect. Biomacromolecules. 2014;15:1019–30.
126. Baker RM, Tseng LF, Iannolo MT, Oest ME, Henderson JH. Self-deploying shape memory polymer scaffolds for grafting and stabilizing complex bone defects: a mouse femoral segmental defect study. Biomaterials. 2016;76:388–98.
127. Bao M, Lou X, Zhou Q, Dong W, Yuan H, Zhang Y. Electrospun biomimetic fibrous scaffold from shape memory polymer of PDLLA-co-TMC for bone tissue engineering. ACS Appl Mater Interfaces. 2014;6:2611–21.
128. Chen C, Hu J, Huang H, Zhu Y, Qin T. Design of a Smart Nerve Conduit Based on a shape-memory polymer. Adv Mater Technol. 2016;1:1600015.
129. Kai D, Tan MJ, Prabhakaran MP, Chan BQY, Liow SS, Ramakrishna S, et al. Biocompatible electrically conductive nanofibers from inorganic-organic shape memory polymers. Colloids Surf B Biointerfaces. 2016;148:557–65.
130. Chan BQY, Liow SS, Loh XJ. Organic–inorganic shape memory thermoplastic polyurethane based on polycaprolactone and polydimethylsiloxane. RSC Adv. 2016;6:34946–54.
131. Castillo-Cruz O, Aviles F, Vargas-Coronado R, Cauich-Rodriguez JV, Chan-Chan LH, Sessini V, et al. Mechanical properties of l-lysine based segmented polyurethane vascular grafts and their shape memory potential. Mater Sci Eng C Mater Biol Appl. 2019;102:887–95.
132. Chan-Chan LH, Tkaczyk C, Vargas-Coronado RF, Cervantes-Uc JM, Tabrizian M, Cauich-Rodriguez JV. Characterization and biocompatibility studies of new degradable poly(urea) urethanes prepared with arginine, glycine or aspartic acid as chain extenders. J Mater Sci Mater Med. 2013;24:1733–44.
133. Lendlein A, Langer R. Biodegradable, elastic shape-memory polymers for potential biomedical applications. Science. 2002;296:1673–6.
134. Bodaghi M, Damanpack AR, Liao WH. Adaptive metamaterials by functionally graded 4D printing. Mater Des. 2017;135:26–36.
135. Bai Y, Jiang C, Wang Q, Wang T. A novel high mechanical strength shape memory polymer based on ethyl cellulose and polycaprolactone. Carbohydr Polym. 2013;96:522–7.
136. Joo YS, Cha JR, Gong MS. Biodegradable shape-memory polymers using polycaprolactone and isosorbide based polyurethane blends. Mater Sci Eng C Mater Biol Appl. 2018;91:426–35.
137. Jing X, Mi HY, Huang HX, Turng LS. Shape memory thermoplastic polyurethane (TPU)/poly(epsilon-caprolactone) (PCL) blends as self-knotting sutures. J Mech Behav Biomed Mater. 2016;64:94–103.
138. Wischke C, Neffe AT, Steuer S, Lendlein A. Evaluation of a degradable shape-memory polymer network as matrix for controlled drug release. J Control Release. 2009;138:243–50.

139. Alfonso F, Perez-Vizcayno MJ, Ruiz M, Suarez A, Cazares M, Hernandez R, et al. Coronary aneurysms after drug-eluting stent implantation: clinical, angiographic, and intravascular ultrasound findings. J Am Coll Cardiol. 2009;53:2053–60.
140. Chen MC, Chang Y, Liu CT, Lai WY, Peng SF, Hung YW, et al. The characteristics and in vivo suppression of neointimal formation with sirolimus-eluting polymeric stents. Biomaterials. 2009;30:79–88.
141. Musial-Kulik M, Kasperczyk J, Smola A, Dobrzynski P. Double layer paclitaxel delivery systems based on bioresorbable terpolymer with shape memory properties. Int J Pharm. 2014;465:291–8.
142. Yan K, Xu F, Li S, Li Y, Chen Y, Wang D. Ice-templating of chitosan/agarose porous composite hydrogel with adjustable water-sensitive shape memory property and multi-staged degradation performance. Colloids Surf B Biointerfaces. 2020;190:110907.
143. Lendlein A, Steuer S, Tuleweit A. Systems for releasing active ingredients based on biodegradable or biocompatible polymers with a shape memory effect: International Publication; 2004. p. 006885.
144. Landsman TL, Touchet T, Hasan SM, Smith C, Russell B, Rivera J, et al. A shape memory foam composite with enhanced fluid uptake and bactericidal properties as a hemostatic agent. Acta Biomater. 2017;47:91–9.
145. Fang Y, Xu Y, Wang Z, Zhou W, Yan L, Fan X, et al. 3D porous chitin sponge with high absorbency, rapid shape recovery, and excellent antibacterial activities for noncompressible wound. Chem Eng J. 2020;388
146. Tan L, Hu J, Huang H, Han J, Hu H. Study of multi-functional electrospun composite nanofibrous mats for smart wound healing. Int J Biol Macromol. 2015;79:469–76.
147. Yakacki CM, Shandas R, Safranski D, Ortega AM, Sassaman K, Gall K. Strong, tailored, biocompatible shape-memory polymer networks. Adv Funct Mater. 2008;18:2428–35.
148. Zhao W, Zhang F, Leng J, Liu Y. Personalized 4D printing of bioinspired tracheal scaffold concept based on magnetic stimulated shape memory composites. Compos Sci Technol. 2019;184
149. Shadduck JH. Implants for treating ocular hypertension, methods of use and methods of fabrication, vol. 0193095: United States Patent Application Publication; 2004. p. A1.
150. Mills DM, Meyer DR. Acquired nasolacrimal duct obstruction. Otolaryngol Clin N Am. 2006;39:979–99.
151. Park JY, Lee JB, Shin WB, Kang ML, Shin YC, Son DH, et al. Nasolacrimal stent with shape memory as an advanced alternative to silicone products. Acta Biomater. 2020;101:273–84.
152. Jung YC, Cho JW. Application of shape memory polyurethane in orthodontic. J Mater Sci Mater Med. 2010;21:2881–6.
153. Lendlein A, Behl M, Hiebl B, Wischke C. Shape-memory polymers as a technology platform for biomedical applications. Expert Rev Med Devices. 2010;7:357–79.
154. Kumar A, Han SS. PVA-based hydrogels for tissue engineering: a review. Int J Polym Mater Polym Biomater. 2016;66:159–82.
155. Paonessa S, Barbani N, Rocchietti EC, Giachino C, Cristallini C. Design and development of a hybrid bioartificial water-induced shape memory polymeric material as an integral component for the anastomosis of human hollow organs. Mater Sci Eng C Mater Biol Appl. 2017;75:1427–34.
156. Fisher JG, Sparks EA, Khan FA, Dionigi B, Wu H, Brazzo J 3rd, et al. Extraluminal distraction enterogenesis using shape-memory polymer. J Pediatr Surg. 2015;50:938–42.
157. Ortega JM, Small W, Wilson TS, Benett WJ, Loge JM, Maitland DJ. A shape memory polymer dialysis needle adapter for the reduction of hemodynamic stress within arteriovenous grafts. IEEE Trans Biomed Eng. 2007;54:1722–4.
158. Shandas R, Yakacki Christopher M, Nair Devatha P, Gall K, Lyons M. Shape memory polymer-based transcervical device for permanent or temporary sterilization, vol. 115208: International Publication; 2007. p. A2.

159. Huang WM, Song CL, Fu YQ, Wang CC, Zhao Y, Purnawali H, et al. Shaping tissue with shape memory materials. Adv Drug Deliv Rev. 2013;65:515–35.
160. Miao S, Castro N, Nowicki M, Xia L, Cui H, Zhou X, et al. 4D printing of polymeric materials for tissue and organ regeneration. Mater Today (Kidlington). 2017;20:577–91.
161. Ogawa Y, Ando D, Sutou Y, Koike J. A lightweight shape-memory magnesium alloy. Science. 2016;353:368–70.
162. Liu J, Lin Y, Bian D, Wang M, Lin Z, Chu X, Li W, Liu Y, Shen Z, Liu Y, Tong Y, Xu Z, Zhang Y, Zheng Y. In vitro and in vivo studies of Mg-30Sc alloys with different phase structure for potential usage within bone. Acta Biomater. 2019;98:50–66.
163. Ma P, Hristova-Bogaerds D, Goossens J, Spoelstra A, Zhang Y, Lemstra P. Toughening of poly (lactic acid) by ethylene-co-vinyl acetate copolymer with different vinyl acetate contents. Eur Polym J. 2012;48:146–54.
164. Xiao Y, Qu M, Shi X. Studies on shape memory effect of polynorbornene/poly (lactic acid) blends. Acta Polym Sin. 2018;3:402–9.
165. Espinha A, Guidetti G, Serrano MC, Frka-Petesic B, Dumanli AG, Hamad WY, Blanco A, López C, Vignolini S. Shape memory cellulose-based photonic reflectors. ACS Appl Mater Inter. 2016;8:31935–40.
166. Fan K, Huang W, Wang C, Ding Z, Zhao Y, Purnawali H, Liew K, Zheng L. Water-responsive shape memory hybrid: design concept and demonstration. Express Polym Lett. 2011;5:409–16.
167. Wang CC, Huang WM, Ding Z, Zhao Y, Purnawali H. Cooling−/water-responsive shape memory hybrids. Compos Sci Technol. 2012;72:1178–82.
168. Shayan M, Chun Y. An overview of thin film nitinol endovascular devices. Acta Biomater. 2015;21:20–34.
169. Chun Y, Lin PY, Chang HY, Emmons MC, Mohanchandra K, Levi DS, Carman GP. Modeling and experimental analysis of the hyperelastic thin film nitinol. J Intell Mater Syst Struct. 2011;22:2045–51.
170. Alwade FH, Ismail IJ, Ibrahim FJ. Zirconia in dental and other biomedical applications: An overview. Health Sci J. 2019;8:30–7.